Characterization of healthy and diseased human ascending aorta tissue

By

Nusrat Zabeen Choudhury

Department of Chemical Engineering

McGill University, Montreal, Québec

October 5th, 2005

A thesis submitted to McGill University in partial fulfillment of the requirements of the degree of Master of Engineering.

Your file Votre référence
ISBN: 978-0-494-22638-4
Our file Notre référence
ISBN: 978-0-494-22638-4

ABSTRACT

Little information is available on the structure or mechanical properties of the human ascending aorta (AA). Most studies to date have assumed homogeneous tissue mechanical properties. The objective of this study was to investigate the local variation in AA tissue structure and mechanics. Healthy and pathologic tissue samples of human AA were obtained at autopsy and surgical pathology. Each aortic ring was sectioned into quadrants; anterior, posterior, medial (inner curvature) and lateral (outer curvature). Samples from each quadrant were processed for histological analysis and biaxial tensile testing. The results from this study indicate that regional differences are present in both healthy and diseased human AA tissue. Overall, the medial quadrant contained significantly more elastin and mechanically, it was the thickest, least stiff and most likely to fail in comparison to the other quadrants. The assumption of homogeneity in AA tissue properties may not be a valid one.

RÉSUMÉ

Peu d'informations sont disponibles sur la structure et les propriétés mécaniques de l'aorte ascendante (AA) humaine. La plupart des études sur les propriétés mécaniques ont considéré le tissu comme étant homogène. L'objectif de cette étude était d'étudier la variation locale de la structure du tissu avec les propriétés mécaniques. Des tissus sains et pathologiques de l'AA humaine ont été obtenus lors d'autopsie et de chirurgie. Chaque anneau aortique a été divisé en quatres parties: antérieure, postérieure, médiane (petite courbure) et latérale (grande courbure). Le tissu a été traité pour l'analyse histologique et a subit des tests de tension biaxiales. Les résultats indiquent que les différences régionales sont présentes dans les tissus sains et pathologiques de l'AA humaine. La partie médiane a plus d'élastine, est plus épais, plus élastique et plus susceptible de se déchirer que les autres quarts. Le tissu de l'AA ne doit pas être considéré comme étant homogène.

ACKNOWLEDGEMENTS

I would like to give sincere thanks to my supervisor, Dr. Richard L. Leask (sir), for his advice, financial aid and contagious enthusiasm throughout the duration of my Master's degree. He exposed me to a completely new area of research in chemical engineering at McGill for my graduate studies and made every daunting task that arose from being his first student appear easy to surmount. I would also like to thank Dr. Mongrain, Dr. Cartier, Dr. Butany and Dr. Bouchot for their efforts in making this opportunity possible and for their excellent advice and insight on subject matter that I previously had little knowledge of.

I must also acknowledge the daily help and contributions from all of the co-workers on the 7th floor, especially Monica and Léonie who have been present from start to finish. Everyone was always ready to answer questions and help out. Also, thank you for provided so many fun experiences throughout. Nic, thank you for being intelligently curious, for listening to me and understanding me during my stressful periods. Thanks to my family for allowing me to pursue my studies and for all of the support. To all my friends, to my girls, you all are a great crew.

TABLE OF CONTENTS

LIST OF FIGURES

LIST OF TABLES

LIST OF SYMBOLS

AA	ascending aorta
AAE	annuloaortic ecstasia
AD	aortic dissection
ANOVA	analysis of variance
AS	aortic sinus
AVR	aortic valve replacement
BAV	bicuspid aortic valve
C	collagen
c_1, c_2, c_3	material parameters
D	displacement
E	elastin
ECM	extracellular matrix
E_e	low stress local moduli
E_{ec}	high stress local moduli
E_{ij}	Green's strain
F	force
Ic, IIc, IIIc	deformation invariants
L	dynamic length
L_o	initial length
LVOT	left ventrical outflow tract
MMP	matrix metalloproteinase
Q	polynomial SEF
r	radial direction
SD	standard deviation
SEF	strain energy function
SMCs	smooth muscle cells
T	dynamic thickness
TAV	tricuspid aortic valve
T_o	initial thickness
W	strain energy function
z	axial direction
°C	degrees Celcius
ε	strain
θ	circumferential direction
λ	extension ratio
σ	stress
σ_{ij}	Cauchy stress

1. LITERATURE REVIEW

1.1. THE ASCENDING AORTA

The ascending aorta (AA) is the primary artery of the circulatory system; responsible for distributing blood to the body. The AA begins at the valve sinus, where the coronary arteries that supply blood to the myocardium of the heart are located (Figure 1.1). This blood vessel serves as the conduit for blood exiting through the left ventricle outflow tract (LVOT). As a result, the biomechanics within the AA characterize the pressure and flow for the entire vascular system. It is uniquely constructed to withstand the large fluid and tissue stresses occurring in the LVOT. In an average lifetime, the AA must absorb the stresses associated with billions of heartbeats and simultaneously transport hundreds of millions of litres of blood to the body [1]. During the cardiac cycle, it has, on average, a 10% variation in diameter [2] and can experience a 5-10% stretch along the length of the vessel due to the movement of the heart [3]. It is the structure of the AA, a highly elastic artery with a diameter of 2-3 cm, that allows it to absorb the majority of cardiac load and redistribute this energy to ensure adequate diastolic pressure and blood flow to the coronary arteries [4].

Figure 1.1: The ascending aorta (AA) begins as the aortic sinus (AS) where the coronary arteries are located.

Arteries are blood vessels whose structure consists of three layers. The thickest layer, the *tunica media* defines the mechanical properties of the tissue. It is mainly composed of circumferentially arranged vascular smooth muscle cells (SMCs) and collagen within concentric wavy elastin layers (Figure 1.2) [5]. The inner monolayer of endothelial cells, the majority of the *tunica intima* in healthy vessels, serves to contact the blood running through the artery. The *tunica adventitia* is the outer layer that is composed of fibrous networks of collagen; it dictates the strength of the aortic wall.

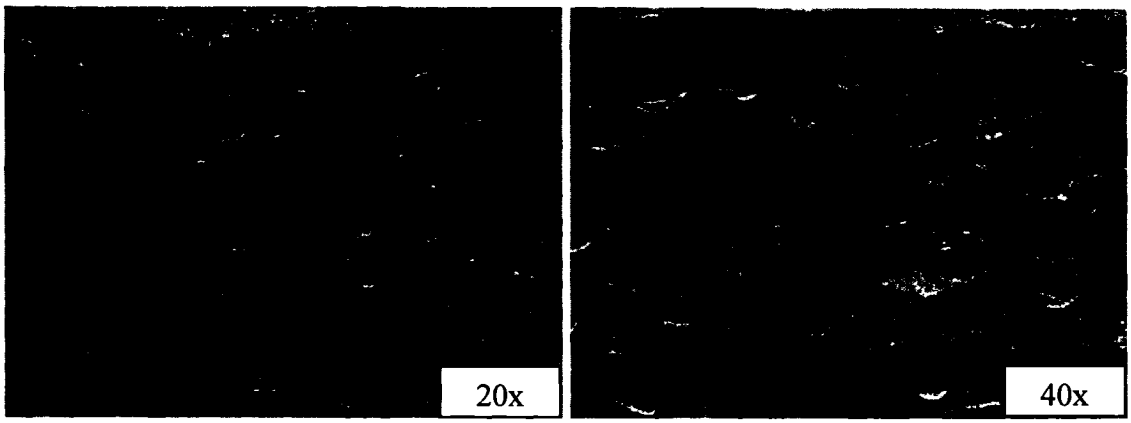

Figure 1.2: Histology image (20x and 40x magnification respectively) of a healthy AA medial layer with elastin (wavy black lamellae), smooth muscle cells (SMCs, red) and collagen bundles (yellow).

The major structural components of aortic tissue are elastin, collagen, SMCs and mucopolysaccharides (Table 1.1) [6]. The structural components of the aortic wall possess the biomechanical properties required to satisfy the physiological requirements of the blood vessel. The flow of blood from the heart is pulsatile. The AA must be flexible to accommodate the varying pressures exerted by the blood that is being pumped rhythmically from the heart. Elastin contributes to the resiliency of the aorta due to a high degree of cross-linking between its monomers. However, it is also a molecule with limited tensile strength and thus additional strength is required to prevent the wall from bursting. It is the collagen fibres (predominantly type IV) of the adventitia that reinforce the tissue to prevent over-expansion. Collagen derives strength from its structure: a

stable triple helix. SMCs are the components that contribute to the active response; SMC contraction and relaxation is usually a continuous sustained state that is triggered by neurohormonal stimuli [7]. Furthermore, the SMCs are believed to be the major secretors of the extracellular matrix (ECM) [8]. The mucopolysaccharides are fibrous, long chain polymers of amino acid sugars. They possess ionic groups that have an important effect on the interstitial pressure of the vessel [9] and serve as lubrication between components.

Table 1.1: Composition (mean value ± SD) of the major components of healthy human ascending aorta tissue [6].

Component	% Composition
Elastin	24.3 ± 7.7
Collagen	36.8 ± 10.2
SMCs	33.5 ± 10.4
Mucopolysaccharides	5.6 ± 6.7

1.2. MAJOR PATHOLOGIES AND THEIR SIGNIFICANCE

In normal individuals, the AA is a compliant artery that helps to redistribute the energy of the cardiac cycle to augment blood flow in the body. Histologically, the AA is dominated by its elastic media. The healthy media is comprised of highly organized lamellae of elastin, smooth muscle cells with very little collagen or mucopolysaccharides (Figure 1.3A).

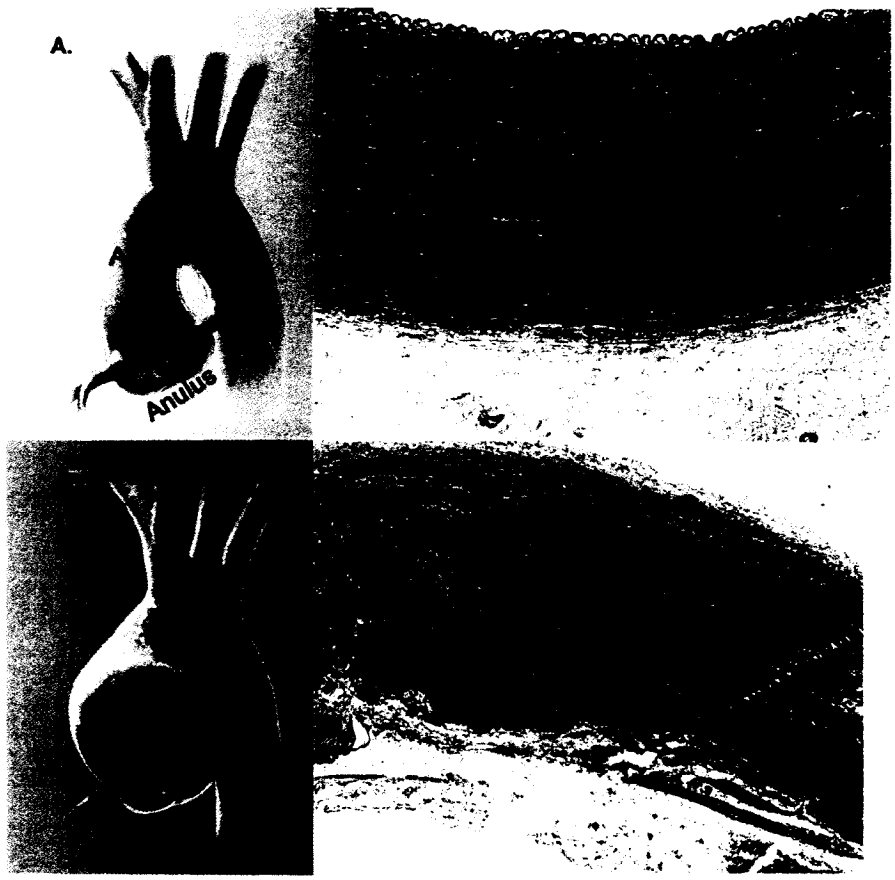

Figure 1.3: Examples of A) healthy AA with an orderly structure of smooth muscle cells and elastic lamellae, B) a connective tissue disorder patient with focal disruption of the elastic lamellae (asterix) and mucopolysaccharide pools (arrow). AA- ascending aorta, AS- aortic sinuses.

1.2.1 Description of Major Pathologies

Changes in the AA dynamics that arise with age and/or disease can lead to cardiovascular complications and death. The importance of proper functioning of the AA is underscored by the high morbidity and mortality rates associated with diseases of the AA. The major aortic pathologies include dissections, aneurysms and atherosclerosis. All of these vascular diseases involve the deterioration of the structural components of the blood vessel wall, referred to as medial degeneration.

Aneurysmal dilatations occur when a blood vessel wall becomes weakened or damaged, and can result in often fatal ruptures or dissection (channeling of blood through the tissue) as the tissue is no longer able to sustain the stresses incurred. Atherosclerosis is a known precursor to dilatation. It can also lead to vessel occlusion and/or dissection. Atherosclerosis is principally a disease of the intima [10]. The disease begins as fibromusclar intimal thickening that can progress to the formation of fibrofatty plaques on the inner layer of the tissue. The affected region of the artery can become narrowed by lesions and can lead to the development of stress concentrations.

Genetic pathologies of the AA also exist. The most prevalent are known as Marfan's syndrome and Ehlers-Danlos syndrome. Both involve mutations of genes that affect connective tissues and result in a change of the mechanical properties of the tissue. The associated medial degeneration is usually patchy, involving focal SMCs loss and elastic fragmentation (Figure 1.3B).

Associated with disease are comorbidities; they can result in consequence of disease and/or can be attributed to the artificial intervention that may be required in treatment. Comorbidities of the AA arise with bicuspid valve disease, annuloaortic ectasia (AAE), bypass surgery and valve surgery (aortic valve replacement and/or Bental procedure). There is a high prevalence of AA dilatation in patients with a bicuspid aortic valve [11]. The combination of AA dilation, dilation of the aortic sinus and annulus is termed AAE, causing aortic valve incompetence and leads to other cardiovascular complications and/or death. Furthermore, cross-clamping that is used in bypass surgery can cause injury to the AA.

1.2.2. Significance of Dilatation

Dilatation of the AA increases the risk of rupture, dissection and concomitant sudden death. It is the most frequent aortopathy requiring surgical treatment [12]. Dilation, caused by the degeneration of the AA medial layer, can lead to aneurysm formation,

dissection or rupture of the AA and is a common cause of aortic valve insufficiency. This occurs in three distinct groups of patient populations: patients with connective tissue disorders, bicuspid valve patients and tricuspid valve patients. The pathogenesis of aortic dilatation is still poorly understood. As a result, the most common treatment remains to replace the AA with a non-compliant Dacron graft which is incapable of restoring "healthy" physiology.

Patients with connective tissues disorders such as Marfan's syndrome or Ehlers-Danlos syndrome are at high risk of AA dilation and rupture. These syndromes are believed to be due to genetic variations that defects the synthesis of fibrillin (a component of elastic tissue) and collagen respectively [13].

Patients with congenitally abnormal (commonly bicuspid) aortic valves (BAVs) are at increased risk of AA dilatation and show evidence of cystic medial change: the focal fragmentation or loss of elastic fibres, loss of smooth muscle cells and accumulation of mucopolysaccarides. The cause of dilated AA with bicuspid patients is still highly controversial. A genetic dysfunction has been hypothesized, however, others believe dilation is due to hemodynamic effects of the bicuspid valve [14-16].

In tricuspid aortic valve (TAV) patients, a number of factors can cause AA dilation. Autopsy studies have shown that asymptomatic aneurysmal dilation (>50% increase in diameter) of the AA occurs in up to 0.6% of the total population over the age of 65 with a tricuspid aortic valve [17]. Dilation of the AA often occurs in combination with the weakening and stretching of the sinuses of Valsalva (aortic sinuses) and aortic annulus, resulting in AAE. The most common causes of AAE are degenerative tissue changes by cystic medial degeneration or atherosclerosis. Both cystic medial degeneration and atherosclerosis are believed to be caused, in part, by hemodynamic forces.

In the past, many surgical procedures have been suggested to correct or prevent the progression of these pathologies [18-22]. Historically, the most popular treatment has

been the replacement of the native aortic valve with a mechanical heart valve and the AA with a synthetic graft. This treatment requires a lifetime of anticoagulation and significantly alters the dynamics of the systemic and coronary circulation. During the last two decades, surgical repair has been proposed in an effort to preserve the physiology of the native aortic valve and improve the hemodynamics of the AA [23;24]. Unfortunately, repair is not always an option and all current treatments for aortic dilatation, including repair, still produce blood flow disturbances and adverse mechanical stresses on the valve leaflets, annulus and aorta. To optimize new surgical treatments and design better prostheses, an understanding of the healthy AA structure and structural consequences of AA dilation must first be realized.

1.3. STRUCTURE AND BIOMECHANICS

The hemodynamics of the AA are determined by the fluid and structural interaction of the LVOT. The aorta is a viscoelastic vessel, and as such its diameter varies with pulse pressure and propagates pressure and flow waves [25]. The structured media of elastic plates and interspersed collagen and smooth muscle cells is responsible for the mechanical properties of the AA. The aorta is a major determiner of vascular compliance, contributing to 60-70% of total systemic compliance [26]. Changes to the medial structure due to age or disease cause corresponding losses of mechanical properties and alterations in peripheral vascular pressure [27;28].

In vivo measures of the elastic modulus and distensibility of the AA from medical imaging devices (CT, MRI and echocardiograms) are now common clinical measures. However, these estimates can only predict the global isotropic mechanical properties within the measured physiologic range [29;30]. *In vitro,* tensile tests have predominantly been used to determine the local mechanical properties of human vascular tissue.

1.3.1. Theoretical Framework of Tensile Tests

Tensile tests are used to quantify the mechanical properties of a material by measuring the deformation characteristics of the material. The force per unit cross-sectional area that produces the deformation is called the stress (equation 1.1) and the deformation (with respect to the original shape) is called the strain (equation 1.2)

$$\sigma = F / A \tag{1.1}$$

$$\varepsilon = \frac{L - L_o}{L_o} \tag{1.2}$$

where F is the force (N), A is the cross-sectional area (mm^2), L is the deformed tissue length (mm) and L_o (mm) is the initial length. A material undergoes elastic deformation if it regains its original shape when the force is removed. If the material retains some or all of the deformation, plastic deformation is experienced. Material characterization from an engineering perspective is usually accomplished by plotting stress versus strain (Figure 1.4). Each material has a unique curve from which mechanical properties can be obtained. Important mechanical properties consist of the modulus of elasticity (flexibility), tensile strength (maximum stress attained) and the yield (load corresponding to the onset of plastic deformation). The yield stress is defined as the stress where the slope of the curve begins to decrease with increasing strain [31]. The tensile strength corresponds to the highest stress value on the curve [31]. Young's modulus of elasticity, corresponds to the slope of the curve prior to the yield point [31]. Young's modulus is used to describe the linear portion of the stress-strain curve and therefore is an elastic property of a given material.

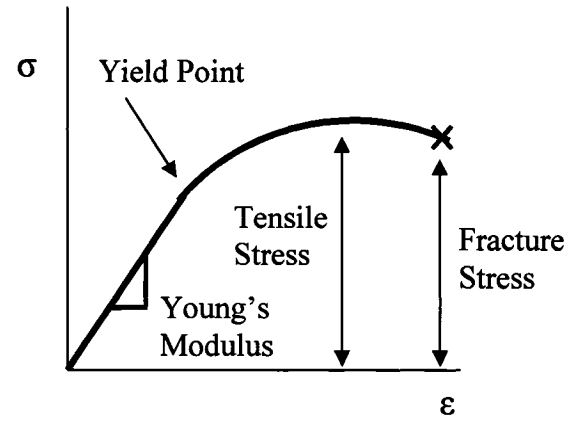

Figure 1.4: Engineering stress-strain curve.

The force required to deform a material of a given yield stress is dependent not only on the amount of deformation required but also on specimen geometry [32]. In the aortic wall, the stress along three directions must be considered: circumferential, axial and radial. Constitutive equations for the AA, used to relate stress to the corresponding state of strain for an elastic material, can thus be quite elaborate; having to relate nine components of stress with nine components of strain. The nine components are illustrated in Figure 1.5; of these σ_{11}, σ_{22} and σ_{33} are the normal stresses that occur along the orthogonal directions of the material and σ_{ij} $(i \neq j)$ are the shearing stresses.

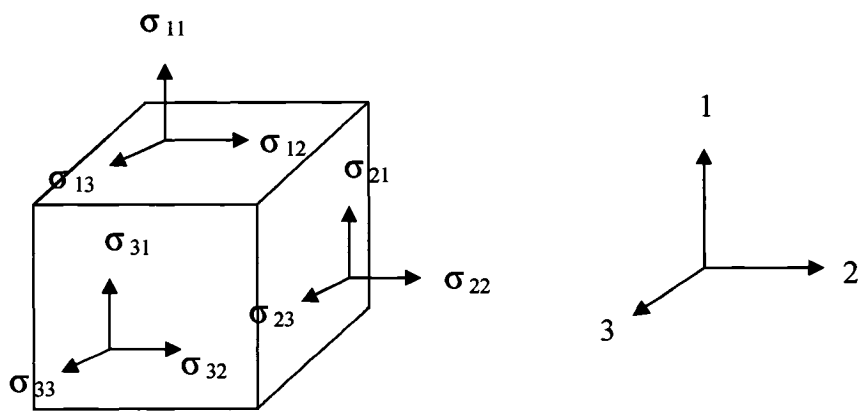

Figure 1.5: The nine components of stress involved in the 3-D mechanical response; nine components of strain are associated with each of these stresses.

The passive biomechanical response of vascular tissue is complex; it depends on the amount of the structural proteins such as collagen and elastin, their interaction and morphological arrangement in the arterial wall [33;34]. The orientation of components in the microstructure of the tissue results in an anisotropic (directionally dependent) response. Uniaxial tensile testing of vascular tissue demonstrates that the mechanical response is non-linear for large strains, which is attributed to the interaction of the structural proteins elastin (compliant) and collagen (stiff). The elastic response is said to be due to elastin for low stress (linear region 1) and the combination of collagen and elastin for high stress (linear region 2), demonstrated in Figure 1.6. Thus the individual contribution of each of the proteins on the elastic response can be noted [31].

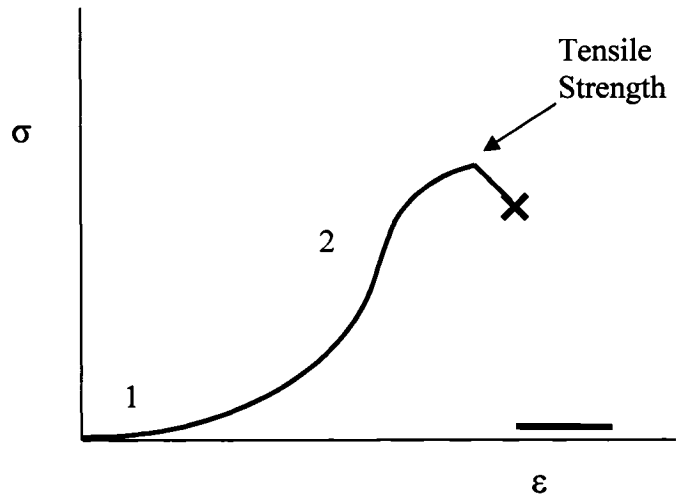

Figure 1.6: Uniaxial vascular stress-strain response for loading of the tissue only. The response is characterized by a low stress and high stress linear regions (1 and 2 respectively).

1.3.2. Viscoelastic Materials

Constitutive models can serve as tools to predict the behaviour of materials in response to applied loads. The familiar constitutive parameter is Young's modulus of elasticity. Young's modulus linearly relates the stress and strain for an elastic material

undergoing small deformations [35]. However, the passive biomechanical response of vascular walls is complex and cannot be described with elastic formulations. Blood vessels are viscoelastic materials; thus behaving with both solid and fluid characteristics. A viscoelastic material displays hysteresis under cyclic loading (loading and unloading stress-strain curves do not coincide), stress relaxation (decrease in stress) under constant strain, creep (slow extension) under constant loads (Figure 1.7). Relaxation and creep cause for the biomechanical response to exhibit time dependence. The stress-strain behaviour is also history dependent and varies with the strain rate or frequency applied [36].

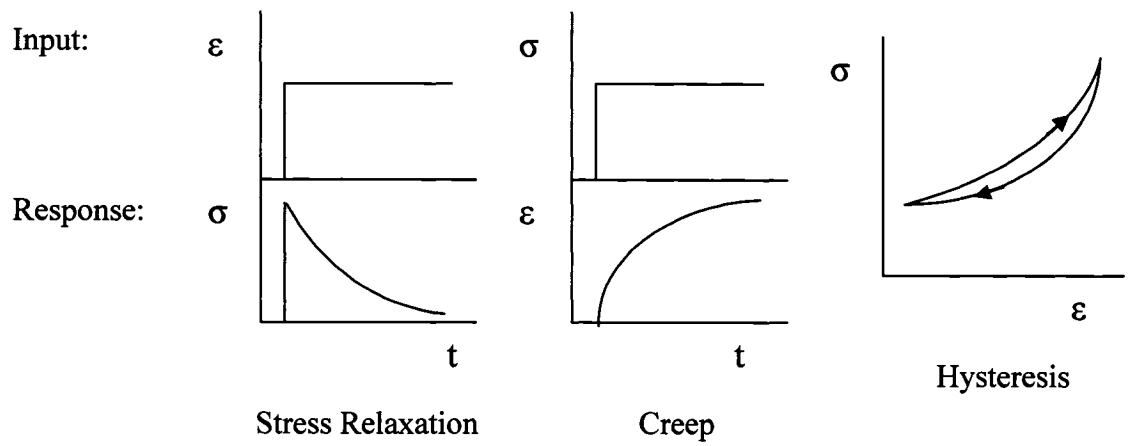

Figure 1.7: Properties of viscoelastic materials (adapted from Callister [37])

1.3.3. Hyperelasticity

The biomechanical response of soft tissues is non-linear for large deformations and thus elastic properties cannot adequately define the behaviour. In the past, investigators have used an incremental analysis, which involves the computation of the mechanical properties along small regions of the stress-strain curve [38]. For small deformations, linear (elastic) deformation can be assumed and thus the entire curve can be characterized with many linear segments with slopes corresponding to incremental Young's moduli. It has been noted that the incremental moduli depend highly on their

reference state and thus, it has been argued that a true incremental analysis is only valid through incremental tests [6]. This method is widely regarded as an acceptable approximation.

The quantification of elastic properties does not capture the non-linear behaviour of the arterial wall. The biomechanics of arteries can instead be described by assuming hyperelastic (inviscid and non-plastic) behaviour; originally used to determine the homogeneous and isothermal behaviour of elastomers. A hyperelastic material stores energy as it deforms. This energy is described as a strain energy function (SEF) annotated as W. These functions are defined in terms of deformation invariants, such as $W(I_C, II_C, III_C)$ as an example. The invariants are composed of the extension ratios (λ_i) that are defined as the deformed and original dimensions respectively of the tissue sample, enabling to reduce the function in terms of three variables instead of the nine variables of strain. Furthermore, these invariants are independent of the coordinate system chosen:

$$I_C = \lambda_1^2 + \lambda_2^2 + \lambda_3^2 \tag{1.3}$$

$$II_C = \lambda_1^{-2} + \lambda_2^{-2} + \lambda_3^{-2} \tag{1.4}$$

$$III_C = \lambda_1^2 \lambda_2^2 \lambda_3^2 \tag{1.5}$$

Investigators have been using this method to approximate the response of biological tissues for large strains since tissues like elastomers can be approximated as incompressible and as such, the product of the three extension ratios is equal to one ($\lambda_1\lambda_2\lambda_3=1$) and the SEF becomes simplified [39]. For a material that is deforming isothermally, stress can be determined directly from a SEF (W), the unique strain energy potential [40]. The model stresses are determined by taking the derivative of the SEF; enabling the stress to be obtained at any given deformation:

$$[S] = \frac{\partial W}{\partial [E]} \tag{1.6}$$

Most investigators have described SEFs for the arterial wall as an exponential (originating from the work of Fung) or a polynomial (adapted from the SEFs used for elastomers) relation [3;41;42]. Constitutive models have been determined for arteries and more specifically, for the aorta; most of which assume incompressibility of the tissue. In addition to the approximation of incompressibility, some models classify the tissue as isotropic so that the elastic parameters of aortic tissue do not vary with direction [43-45]. However, as this is not the case with vascular tissue, recent SEFs tend to include directional properties [46].

Investigators have developed transversely isotropic models that assume that a material has a preferential response in one direction and a different response in all perpendicular directions [47]. Anisotropic models that incorporate the three dimensional response of the tissue have also been established [41;48;49]. Most anisotropic models assume cylindrical orthotropy; the material behaves symmetrically with respect to three orthogonal directions (r, θ, z). It is the Fung-type (exponential form) SEF [50] that has been used most successfully in quantifying the stress-strain behaviour of soft biological tissues. It is

$$W = \mathbf{c}[e^{Q(E)} - 1] \tag{1.7}$$

where **c** is a material parameter and Q is a polynomial that incorporates the principal strains and additional material parameters. The polynomial Q, can be defined to yield an orthotropic, a transverse isotropic, or an isotropic SEF

$$\begin{aligned} Q_{orth} = {} & c_1 E_{11}^2 + c_2 E_{22}^2 + c_3 E_{33}^2 + 2c_4 (E_{11} E_{22}) + 2c_5 (E_{22} + E_{33}) + 2c_6 (E_{33} E_{11}) + \\ & c_7 (E_{12}^2 + E_{21}^2) + c_8 (E_{23}^2 + E_{32}^2) + c_9 (E_{31}^2 + E_{13}^2) \end{aligned} \tag{1.8}$$

$$\begin{aligned} Q_{trans} = {} & c_1 (E_{11}^2 + E_{22}^2) + c_2 E_{33}^2 + 2c_4 (E_{11} E_{22}) + 2c_5 (E_{11} + E_{22}) E_{33} + \\ & c_7 (E_{12}^2 + E_{21}^2) + c_8 (E_{23}^2 + E_{32}^2 + E_{13}^2 + E_{31}^2) \end{aligned} \tag{1.9}$$

$$\begin{aligned} Q_{iso} = {} & c_1 (E_{11}^2 + E_{22}^2 + E_{33}^2) + 2c_4 (E_{11} E_{22} + E_{22} E_{33} + E_{33} E_{11}) + \\ & c_7 (E_{12}^2 + E_{21}^2 + E_{23}^2 + E_{32}^2 + E_{13}^2 + E_{31}^2) \end{aligned} \tag{1.10}$$

The concern arising with the use of SEFs is that although they capture the non-linear response of arteries, many assumptions, such as hyperelastic behaviour and a homogeneous response are often required for their formulation. Many different SEFs have been developed to address inhomogeneity by including both the medial and adventitial [51;52] layer and incorporating the structure [53] of the arterial wall. However, the physical meaning of the constants in the equations remains unclear. Despite these limitations, the use of SEFs is widely popular for describing soft tissue response [53].

1.3.4. Pseudo-elasticity

The viscoelastic nature of the arterial wall can be approximated through pseudo-elastic relations. A viscoelastic material behaves differently in loading and unloading because energy is stored during cyclic perturbations; resulting in what is called a hysteresis loop. When a viscoelastic material is cycled a sufficient number of times, the hysteresis loop becomes repeatable and the material is said to be preconditioned (Figure 1.8). The term pseudo-elastic has been coined by Fung referring to the fact that tissue can be approximated elastic because the response is repeatable. Furthermore, if one treats the response as one elastic material during loading and another in unloading, the entire hysteresis loop can be captured [41]. The resulting constitutive relation describes the stress exhibited by the material at a given strain, provided that it is known whether the material is being loaded or unloaded. This approach can be combined with SEFs to yield hyperelastic pseudo-elastic equations that can model both the loading and unloading curves of the tissue. However, it has been established that aortic tissues exhibit little hysteresis, approximately 5% [54]. Thus, for aortic tissue, the mechanical characterization of only the loading response is sufficient.

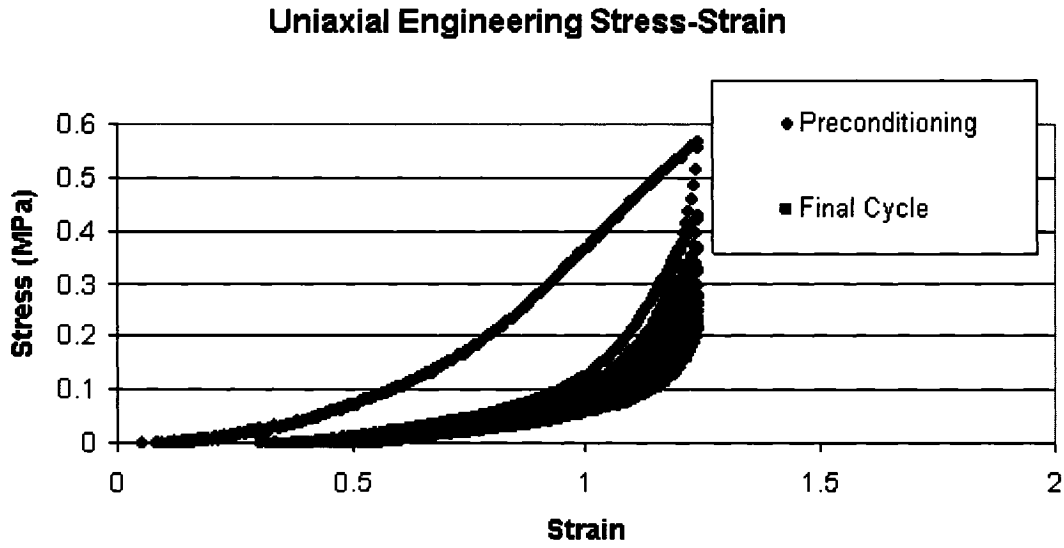

Figure 1.8: Uniaxial engineering stress-strain of human ascending aorta tissue subjected to ten preconditioning cycles (data obtained from preliminary tests performed for this study).

1.4. EXPERIMENTAL STUDIES

1.4.1. Tensile Tests

There exist many methods to obtain experimental stress-strain curves for the AA. There are two categories of tests: *in vivo* and *in vitro.* The first examines the blood vessel within the body by measuring pressure and volume changes along the artery. *In vivo* experimentation has been limited because it is invasive [3]. Furthermore, the data is difficult to apply to an entire blood vessel as there are geometric differences from segment to segment. Thus, there has been a recent focus on *in vitro* experimentation; more specifically, pressure-diameter and tensile testing. In these tests, excised segments of tissue are subjected to engineering-type material testing. The tissue is stretched along one or many orthogonal directions (uniaxial, biaxial or triaxial) and both the stretch and required load is measured.

In vitro experimentation provides the mechanical properties of tissue as a material; however it does not provide insight as to how the tissue responds within the body. To overcome this limitation, many researchers conduct tests by closely simulating physiological settings. The specimens are stored and tested in physiological saline solutions. All tissue segments are initially stretched to their *in vivo* length because it is known that ascending aortic tissue can contract from up to 30-50% upon excision [3]. Static tests employing a fixed strain rate are often executed at body temperature (37 °C). Dynamic tests with cyclic inputs use sine functions to resemble pulse waves with a frequency and amplitude similar to the average human heartbeat and pressures (systolic and diastolic). Active rather than passive tests can also be conducted for either static or dynamic tests by stimulating the SMCs into either a contracted or relaxed state to capture the response of not only the passive response of the structural proteins (elastin and collagen) but the active response of the SMCs as well.

In pressure-diameter testing, tubular segments of blood vessels are used. The tissue is inflated with pressurized saline solution. The pressure and resulting diameter change is recorded and the data is used to generate a pressure-diameter curve from which a pressure-strain elastic modulus can be obtained [55]. Tensile tests consist of attaching the ends of a prepared specimen strip with either sutures or clamps. The material is stretched to its *in vivo* length and preconditioned. A fixed extension rate is applied to the ends of the specimen and the corresponding increase in load is measured. The data from all tests is used to generate a stress-strain curve to which constitutive equations are fit.

1.4.2. Anisotropy and Heterogeneity

Comparisons of the data from uniaxial tensile testing obtained through testing different directions of the tissue have determined that the aortic wall has anisotropic properties (properties that vary with direction) and thus there is a need for biaxial tensile testing [56]. For many soft tissues, a biaxial test is sufficient to characterize the three

dimensional response of the tissue because it can be assumed incompressible. With this assumption, if the response along two directions is known then the third can be determined because the volume of the tissue remains constant. Mohan and Melvin performed biaxial inflation tests on mid-thoracic aortas and discovered that the tissue was most likely to tear and rupture due to stretch in the axial direction [57]. Patel's data revealed that the tissue is cylindrically orthotropic [35]. Biaxial tensile testing, where the response of the crosslinks between the structural components is quantified, demonstrated that vascular tissue behaves non-linearly and is biaxially anisotropic in the physiological range [54].

Although biaxial experimentation has taken into account the anisotropic response of blood vessels, most experimental and theoretical analyses have been limited by assuming homogeneous mechanical properties. There exist a few studies that have investigated the local variation of tissue.

In a study of abdominal aortic aneurysms, Thubrikar *et al.* have shown in a small number of cases (n=5) that regional variations of the mechanical properties of the tissue do exist [58]. Owing to the geometry of the AA it is much more difficult to identify asymmetrical dilations from medical images and gross examination. Some evidence does exist suggesting a prevalent focal nature to AA medial degeneration.

Recently Agozzino *et al.* showed that in patients undergoing surgery for tricuspid valve disease (stenosis, regurgitation or both) medial degeneration does not occur uniformly around the aortic sinuses [59]. The authors looked at two locations in 22 patients corresponding to the non-coronary and right coronary sinus and found that medial degeneration was more severe on the non-coronary sinus side of the AA. It has been hypothesized that the asymmetry in hemodynamic forces in the AA lead to focal medial disruption, yet no study has identified the tissue or fluid stresses in these vessels.

Vorp *et al.* have suggested that the risk of rupture in an abdominal aneurysm is most probably related to the wall stress that the given region experiences [60]. The group

has conducted a study to evaluate the effect of not only the diameter (size) of the aneurysm, but also its shape. Asymmetry in an aneurysm will lead to variances in stress distribution, which could lead to a specific region being more prone to rupture than others.

Ishii and Asuwa have investigated the degradation of fibres in aortic dissection with respect to the expression of matrix metalloproteinases (MMPs) [61]. They stipulate that a segment of the AA made vulnerable through hemodynamic stress, causes SMCs to secrete MMP-2 and MMP-9. MMPs alter the ECM around the SMCs to allow functional changes to the cells, such as proliferation and migration. In medial degeneration, these proteins are over-expressed and cause elastic fibre fragmentation and fibrous thickening. They have shown a regional change in the SMCs and that the basement membrane of the SMCs was sparse or lacking.

Matsumoto *et al.* have suggested that MMP activity plays a major role in the pathogenesis of atherosclerosis [62]. They have stated that the activity of these proteins allows SMCs to migrate from the media to the intima and subsequently agglomerate, forming an intimal lesion. The group has investigated the expression of MMPs through immunochemistry: staining sections of aortic tissue, mounting the specimens on glass slides and then observing at high magnification. Their findings suggest that the simultaneous expression of MMP-2, MMP-9, and MMP-12 is responsible for elastin degradation in atherosclerosis.

Angouras *et al.* studied the importance of the vasa vasorum vessels (found in the adventitia) in the thoracic aorta [63]. In this study, Landrace pigs were subjected to an interruption of vasa vasorum flow to the aorta, by excising the periaortic connective tissue. Histological examination and the evaluation of collagen and elastin content by image analysis were performed. Histology of the aortas revealed ischemic necrosis along with abnormal straightening of the elastin and collagen fibres of the outer medial region. However, the content of collagen and elastin did not significantly change. The borderline between the outer ischemic and inner non-ischemic media was well defined and an outset

of dissection was observed along this region. This study demonstrates that nutrient deprivation results in a regional stress being placed on the aortic wall, which may be an important factor in the onset of dissection.

1.4.3. Current Standing

Although much has been learned about the pathology of aortic disease, past studies have assumed homogeneous and isotropic AA tissue properties. To date almost nothing is known about the heterogeneity of aortic disease. From an engineering standpoint, insufficient mechanical data is available to properly analyze the biomechanics or model the hemodynamics of the human AA. This is due to a total lack of fundamental material property data on healthy and diseased AA. Moreover, to understand the pathogenesis and the role of hemodynamics in the development of AA aneurysms, dissections and AAE requires data on the local variation in tissue structure and biochemistry.

2. OBJECTIVES

The objective of this study is to identify whether regional differences exist in the local properties of both healthy and pathologic human AA tissue (tricuspid, bicuspid and dilated tissue patients) and to compare the different tissue types. Specifically,

1. To identify if regional mechanical properties vary using biaxial tensile tests;
2. To define the local variation in the content of elastin, collagen and SMCs from histological sections.

The information will be used to compare the structure and composition of the tissue with the observed mechanical response.

The hypothesis of this work is that pathologies which affect the LVOT result in focal AA tissue remodeling.

3. MATERIALS AND METHODS

3.1. TISSUE COLLECTION, GROSSING AND STORAGE

All tissue specimens were obtained under informed consent following the guidelines of the Tri-Council Policy Statement (Appendix A). Pathologic AA tissue was acquired from patients scheduled for cardiac surgery at the Montreal Heart Institute, requiring replacement of the AA (due to valvular disease, annulo-aortic ecstasia, atherosclerosis, aneurysms or dissections). Healthy AA tissue was obtained from autopsy from both the MHI and the University Health Network (UHN) Toronto General Hospital. All of the collected tissues were given an anonymous identification number.

A total of 11 surgical samples and 3 autopsy samples for mechanical testing were collected from the MHI and an additional autopsy sample was obtained from the UHN Toronto General Hospital. All of these samples consisted of a tubular section of the AA (Figure 3.1). The tissue was obtained from 9 men and 6 women with ages ranging from 30 to 74 years old, summarized in Table 3.1. Additional tissue was taken from each of the samples for histological processing.

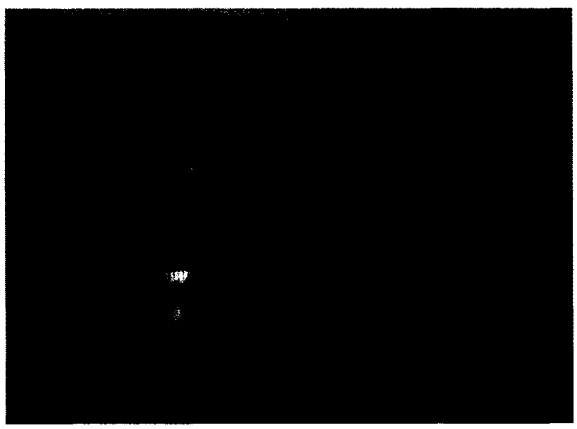

Figure 3.1: Gross photograph of a 42 year old male healthy human AA segment.

Table 3.1: Clinical samples obtained from the Montreal Heart Institute (2-15) and the autopsy sample (1) obtained from University Health Network Toronto General Hospital used for mechanical testing.

Sample #	Age	Sex	Type	Valve Type	Diameter (mm)
1	74	F	Healthy	Tricuspid	30
2	58	M	Pathologic	Bicuspid	50
3	30	F	Healthy	Tricuspid	26
4	55	M	Healthy	Tricuspid	28
5	46	M	Pathologic	Tricuspid	52
6	68	F	Pathologic	Tricuspid	59
7	52	M	Pathologic	Tricuspid	63
8	71	M	Pathologic	Bicuspid	58
9	53	F	Pathologic	Bicuspid	53
10	64	M	Pathologic	Bicuspid	52
11	60	M	Pathologic	Bicuspid	> 50
12	51	M	Pathologic	Tricuspid	42
13	71	F	Healthy	Tricuspid	28
14	66	F	Pathologic	Tricuspid	58
15	44	M	Pathologic	Bicuspid	42

For the histology, additional microscope slides of 18 past surgical samples and 3 autopsy samples were obtained from the UHN and an additional clinical sample was obtained from MHI; resulting in a total of 37 specimens used in the analysis. The additional AA samples were obtained from 18 men and 4 women, with ages ranging from 32 to 83 years old (Table 3.2).

Table 3.2: Additional histological samples obtained. Samples 16-33 and 34-36 are respectively the past surgical samples and the autopsy samples obtained from the (UHN) of the Toronto General Hospital. Sample 37 is the additional sample obtained from the MHI.

Sample #	Age	Sex	Type
16	58	M	Pathologic
17	75	M	Pathologic
18	36	F	Pathologic
19	56	M	Pathologic
20	67	F	Pathologic
21	50	M	Pathologic
22	60	M	Pathologic
23	32	M	Pathologic
24	80	M	Pathologic
25	77	M	Pathologic
26	74	M	Pathologic
27	64	M	Pathologic
28	83	M	Pathologic
29	65	M	Pathologic
30	66	M	Pathologic
31	70	M	Pathologic
32	76	M	Pathologic
33	48	M	Pathologic
34	51	M	Healthy
35	73	F	Healthy
36	73	M	Healthy
37	54	M	Pathologic

The excised tissue was placed in Krebs-Ringer buffer solution and transferred to the biomechanics laboratory. The solution (2L) was prepared by mixing two jars of the powdered medium (Sigma-Aldrich) was added to 90% of the water (1.8 L) at room temperature. The composition of the powder, weighing 9.5 g per jar, is provided in Table 3.3. The medium was dissolved with gentle agitation using a magnetic stirrer plate and bar. Sodium bicarbonate, in the weight of 2.52 g (1.26 g per L of solution) was also added and dissolved. The remaining water was then added to bring the solution to its final volume.

Table 3.3: Composition of a jar of Krebs-Ringer powdered medium (9.5 g) from Sigma-Aldrich.

Components	**g/L**
D-Glucose	1.8
Magnesium Chloride [Anhydrous]	0.0468
Potassium Chloride	0.34
Sodium Chloride	7.0
Sodium Phosphate Dibasic [Anhydrous]	0.1
Sodium Phosphate Monobasic [Anhydrous]	0.18

The intact specimen was grossed by taking digital pictures of the specimen, measuring the proximal and distal diameter of the aortic ring and noting the presence of, if any, remarkable features (such as atherosclerotic lesions). The tissue was then placed in the Krebs-Ringer solution in a closed container and refrigerated at 4°C.

3.2. TISSUE PREPARATION

The tissue sample was placed on a surgical table, oriented such that the proximal end was located below the distal end (Figure 3.2). In this position, the quadrants are

identified as the front quadrant as the anterior, the back quadrant as the posterior, the quadrant on right (the smallest section) as the medial and the quadrant to the left (the largest section) as the lateral. Using dissection scissors, representative tissue samples of the medial (A), anterior (B), lateral (C) and posterior (D) quadrants were then taken. The tissue was cut into square 1.5 cm by 1.5 cm samples with the edges were aligned with the circumferential and axial directions of the aorta.

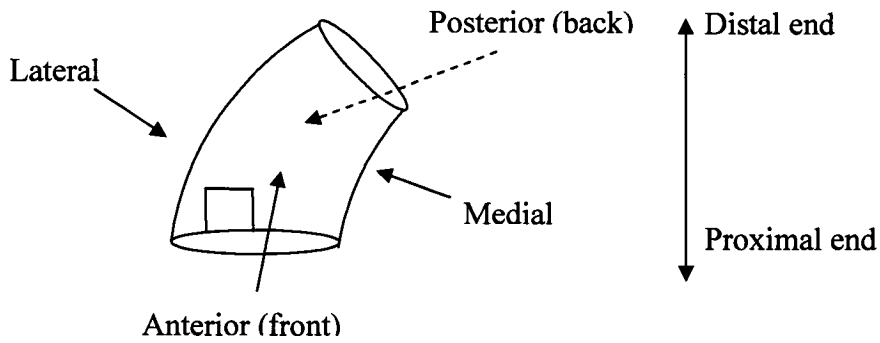

Figure 3.2: Identification of the quadrants in an aortic ring. The square representing the 1.5 x 1.5 cm tissue sample tested.

Each piece was placed in a separate, labeled dish filled with Krebs-Ringer solution at room temperature. India ink (Fisher Scientific) was applied along a circumferential edge to mark its orientation. This procedure is illustrated in Figure 3.3 and an example of the sample pieces obtained is shown in Figure 3.4. When the excised sample was large enough, both proximal and distal pieces were taken from each quadrant. To differentiate between these pieces, red India ink was used to mark proximal pieces and green for distal.

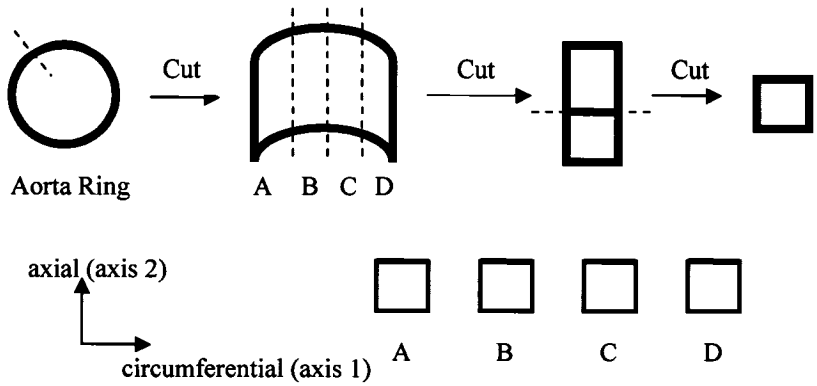

Figure 3.3: Obtaining representative pieces from each quadrant in an aortic ring.

Figure 3.4: Sample pieces taken from each quadrant of an aortic ring.

The dimensions of the samples were taken and recorded using an electronic digital caliper (± 0.01 mm). Three measurements were taken of each of the circumferential and axial lengths and the thickness of the sample and averaged.

As mentioned previously, an additional piece of tissue (0.5 x 1.5 cm) adjacent to each sample was also taken for histological analysis (Figure 3.5). This piece of tissue was placed in a histology cassette labeled with the patient identification number and the quadrant it was taken from. The cassette was then placed in a closed container filled with 4% neutral buffered formalin solution to fix the tissue.

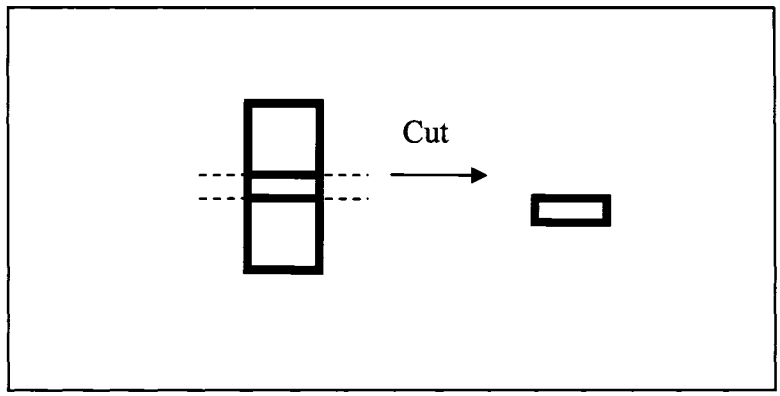

Figure 3.5: Taking a sample of tissue for histological analysis.

3.3. TENSILE TEST METHODS

The AA specimens were subjected to tensile testing with a constant strain rate using the EnduraTEC *elf*® 3200 biaxial tensile tester system supplied with WinTest® software (Figure 3.6).

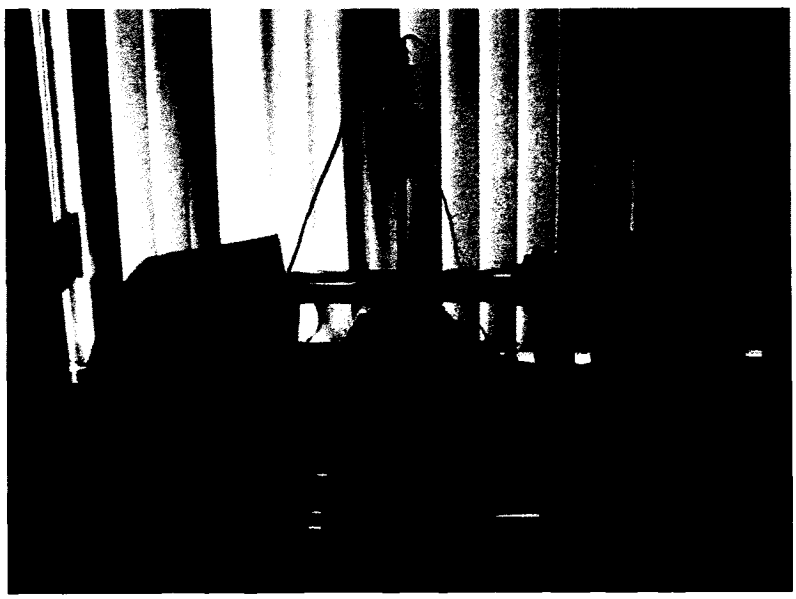

Figure 3.6: EnduraTEC *elf*® 3200 biaxial tensile tester.

3.3.1. Biaxial Tensile Tester

The EnduraTEC *elf*® 3200 system is equipped with 2 load cells and 2 displacement transducers (one for each axis) to measure the force required to displace the axes to which tissue is attached. The system is also accessorized with an optical strain extensometer. This device uses digital video tracking to monitor the displacement of the tissue itself throughout the duration of the test. The specifications for the equipment are provided in Table 3.4. The tissue was attached to the axes with the use of suture grips and floated in a saline bath at room temperature.

Table 3.4: EnduraTEC *elf*® 3200 system specifications.

Load Cell	
Capacity	± 225 N
Percent Error	< 0.5% of Full Scale Range (0.05V in a 0-10V range)
Digital Resolution	1 part in 32768 (0.000305V in a 0-10V range)
Displacement Transducer	
Stroke	± 6.50 mm
Percent Error	< 0.5% of Full Scale range (0.05V in a 0-10V range)
Digital Resolution	1 part in 32768 (0.000305V in a 0-10V range)
Optical Extensometer	
Focal Width	12 to 50 mm
Resolution	0.002 mm at 12 mm focal width
Update Rate	5 Hz
Operation	Static tests or 1 Hz waveform frequency (max)

3.3.2. Tensile Testing Sample Preparation

The specimen was attached to the tester with sutures. Using 3-0 (0.2 mm diameter) silk sutures with pledgets, the suture needle was passed through the adventitial corner edge of the specimen until the pledget (used as reinforcement) was put in place. The second needle located at the other end of the suture is then passed through the tissue approximately 0.3 cm away. The suture needles and excess thread are cut off. The ends are tied into a loop that is 80 mm in length. This procedure is repeated so that there are two loops for every edge of the specimen (Figure 3.7).

Figure 3.7: Suturing tissue specimen with pledgets. A) the top surface and B) the bottom surface with the pledgets.

The specimen (intimal side facing up) is attached to the biaxial grips of the tester by passing each loop around the roller and threading the suture into the roller groove (Figure 3.8). The specimen is oriented so that the circumferential edge is aligned with the primary axis of the tester. The Krebs-Ringer saline solution is poured into the stainless steel bath to level indicated (approximately 1.5 L) as demonstrated in Figure 3.9.

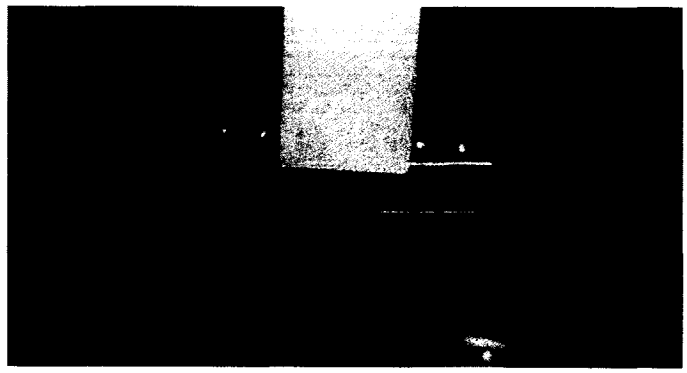

Figure 3.8: Tensile tester suture grips. Each grip has two posts onto which the sutures are wrapped around.

Figure 3.9: Tensile tester stainless steel saline bath. Samples were floated in room temperature Krebs-Ringer solution.

Using a toothpick and green India ink (for high resolution), 4 dots were painted as a central square mark (0.3 cm x 0.3 cm) on the intimal surface of the sample (Figure 3.10). These dots are first identified by the software by placing boxes around them. At this point the position of the dots corresponds to the reference state of zero strain. The points are then tracked by the optical strain extensometer.

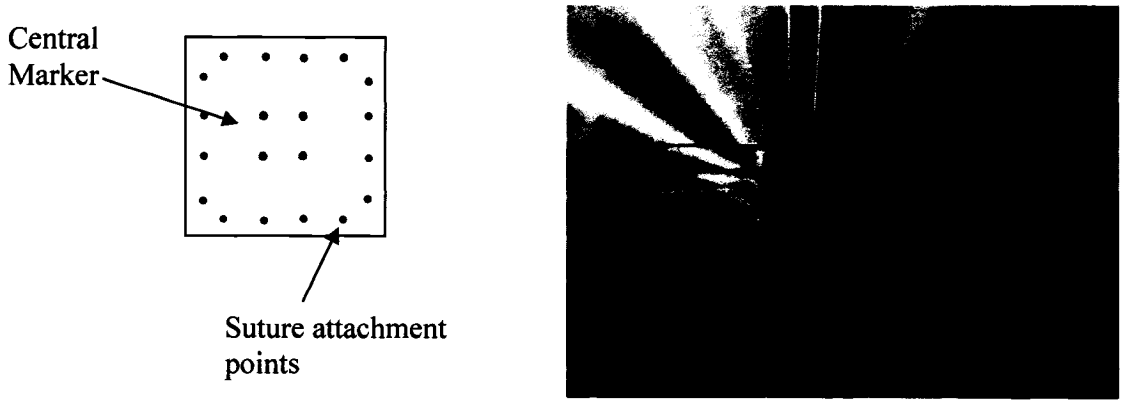

Figure 3.10: Central marker (0.3 cm x 0.3 cm) used for tracking by the optical strain extensometer.

3.3.3. Tensile Test Description

The biaxial tensile tests were conducted on 15 mm x 15 mm pieces of human aortic specimens obtained from each quadrant of a ring of tissue (Section 3.2). Porcine aorta was used to determine the optimal strain rate, number of preconditioning cycles and degree of extension to be used. The developed equi-biaxial test consisted of repeatedly loading and unloading the tissue at a rate of 0.1 mm/sec from a passive equilibrium state (no load) to a 5 mm stretch for 10 preconditioning cycles. These cycles were used to produce a repeatable stress-strain relationship and were immediately followed by 3 experimental cycles. A final stretch of 12 mm (maximum allowed by the tester) was imposed on the tissue. This last stretch was used to obtain the high stress and failure properties of the tissue and the data obtained from the experimental runs will be used in future work to formulate constitutive relations. The load cell, transducer and video extensometer readings were monitored and recorded using WinTest 2.56 software. The data was then imported into Microsoft Excel where the data was analyzed.

Table 3.5: Equi-biaxial tensile testing protocol (starting position at -6 mm).

Index	Command
1	Ramp at 0.1 mm/sec to -6 mm
2	Ramp at 0.1 mm/sec to -1 mm
3	Ramp at 0.1 mm/sec to -6 mm
4	Repeat 13 times starting at index 2
5	Ramp at 0.1 mm/sec to 6 mm

Once the test was completed, the sample was removed from the grips. The sutures and pledgets were cut out of the tissue.

3.4. HISTOLOGY METHODS

A representative tissue sample from each quadrant was prepared for histological analysis. The media is the layer of the aortic wall that is responsible for the mechanical properties of the AA. The passive mechanical response of the tissue is largely dependent on both the amount and the arrangement of elastin, collagen and smooth muscle cells within this layer. Thus, the histological analysis quantified the structure and composition of the medial layer only.

3.4.1. Microscope Slide Preparation

Histology slides were processed by the histology department at the MHI. The slides were prepared from the fixed tissue in formalin. The tissue was embedded in paraffin wax so that thin sections (approximately 3μm) could be cut for mounting onto microscope slides. The specimens were then stained with the Movat Pentachrome stain so that the different components of the tissue could be distinguished (Table 3.6) [64].

Table 3.6: Expected results using the Movat Pentachrome stain [64].

Component	Colour
Nuclei	Blue Black
Elastic Fibres	Black
Fibrin	Red
Muscle	Red
Collagen	Yellow
Mucopolysaccharides	Blue Green

3.4.2. Regional Image Analysis

For a given surgical sample, 4 slides were processed (one for each quadrant of tissue). Comparison of these quadrants allowed for characterization of the tissue composition along the circumference of the tissue. In addition, each slide was divided into equal thirds from the area closest to the intima to the area closest to the adventitia to allow for radial analysis. This method is outlined in Figure 3.11. Finally, the slide was divided into three equal regions for replicate readings.

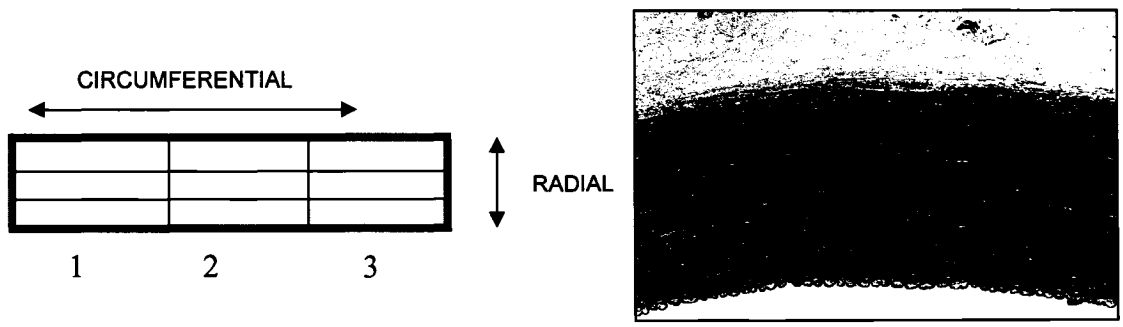

Figure 3.11: Regional analysis of a microscope slide. Replicate readings obtained from regions 1, 2 and 3. I: intimal, B: middle, A: adventitial.

The slides were examined with a Leitz Diaplan upright microscope through a 40x objective. Digitized images were obtained with a Leica DC 300 digital camera affixed onto the microscope. The images were analyzed using a colour detection program written in MATLAB. The program counted the number of pixels present for a given colour range over the total amount of pixels present; yielding a semi-quantitative estimate for the percent composition of a component. For each patient, areas of known content were used to set the colour threshold for each component. The components of interest were elastin (black), collagen (yellow) and SMCs (red) as depicted in Figure 3.12.

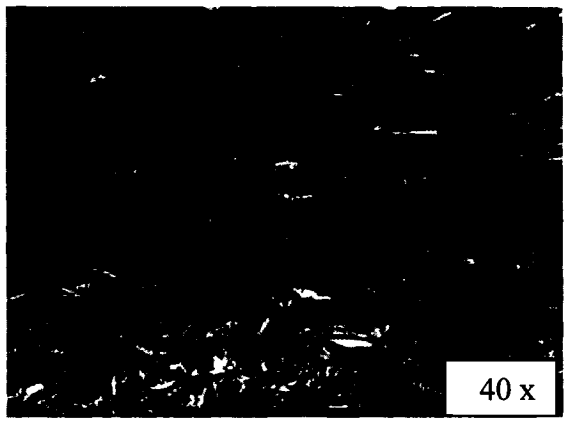

Figure 3.12: Movat pentachrome stain was used to distinguish elastin (black), collagen (yellow) and smooth muscle cells (red). This picture is an example of one of nine taken for a given histological slide; this one is from the anterior quadrant for the region closest to the adventitia.

3.5. STATISTICAL ANALYSES

Statistical analyses were carried out using GraphPad Prism version 4.01 (GraphPad Software, San Diego, California). All statistics are presented as mean values ± standard deviation (SD). In the analyses involving one grouping variable, one way analysis of variance (ANOVA) was used if more than 2 groups were present and t-tests were used if only 2 groups were present. Analyses involving two grouping variables were conducted using two way ANOVA. Bonferroni's multiple comparisons post tests

were used to identify which groups were significantly different with P values <0.05 considered statistically significant. The spread of the data sets was illustrated with Box and Whisker plots by displaying the upper-quartile, inter-quartile and lower-quartile range (25%, 50% and 75%, respectively).

4. RESULTS: BIAXIAL TENSILE TESTS

For the tensile tests, 11 surgical samples of pathologic tissue and 4 samples from autopsy of healthy tissue were used (Table 3.1). These samples consisted of a tubular section of the AA removed during surgery (Figure 3.1). The pathologic samples were sub-grouped by aortic valve type (BAV/TAV) and also regrouped if the aorta was dilated (Ø > 50 mm, includes both BAV and TAV types). The aim was to investigate whether the aortic valve type or the degree of dilation influenced the changes in the circumferential mechanical response of pathologic tissue in comparison to healthy tissue. Table 4.1 summarizes these groups.

Table 4.1: Patient characteristics for biomechanical analysis. Pathologic tissue was grouped according to aortic valve type (BAV/TAV) and also as dilated for comparisons with healthy tissue. BAV: bicuspid aortic valve and TAV: tricuspid aortic valve.

	Tissue Type			
	Healthy	**Pathologic**		
Patient Characteristics	TAV (n=4)	BAV (n=6)	TAV (n=5)	Dilated (n=9)
Mean Age	58 ± 20	57 ± 10	58 ± 9	60 ± 8
Male/Female	1/3	5/1	3/2	6/3

4.1. VARIATION IN TISSUE THICKNESS

The stresses that are incurred on the tissue are highly dependent on its thickness. As a result, any variation in thickness between the quadrants would result in regional variation in the mechanical properties. Three types of analyses were conducted. The first lumped all of the tissue together to look into the general population tissue thickness characteristics using one way ANOVA. The second analyzed the characteristics of a given tissue type (healthy, pathologic tricuspid, pathologic bicuspid and dilated) using

one way ANOVA. Finally, thickness variations between tissue types were compared using two way ANOVA. All statistics are presented as mean values ± standard deviation and P values <0.05 were considered statistically significant.

4.1.1. All Samples

The mean values for the tissue thickness of each quadrant for all of the samples are summarized in Table 4.2. When all of the tissue samples were lumped together, significant differences (P=0.018, one way ANOVA, Bonferroni post test) were detected in the quadrant wall thicknesses between the medial vs. the lateral and posterior quadrants (Figure 4.1). The medial quadrant contains the thickest tissue.

Table 4.2: Mean tissue thickness ± SD for each quadrant for all samples.

	Quadrant			
	Medial	Anterior	Lateral	Posterior
Thickness (mm)	2.01 ± 0.36	1.94 ± 0.35	1.87 ± 0.25	1.85 ± 0.25

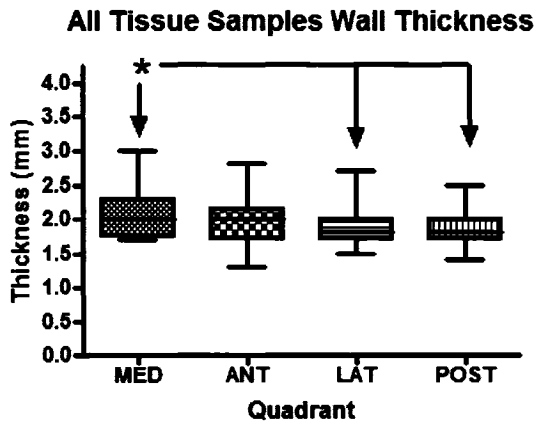

Figure 4.1: AA wall thickness comparison between the quadrants for all tissue. The medial quadrant is significantly thicker that the lateral and posterior quadrants. MED: medial, ANT: anterior, LAT: lateral and POST: posterior quadrants.

4.1.2. Tissue Type

In the comparisons of wall thickness of the tissue based on tissue type, significant differences in the quadrant wall thicknesses were detected for the healthy tissue only (P=0.0046, one way ANOVA, Bonferroni post test), the thickness of the medial quadrant is significantly greater than that of the lateral quadrant (Figure 4.2). Although the analysis of pathologic tissue types did not detect any significant variation, similar trends were noted.

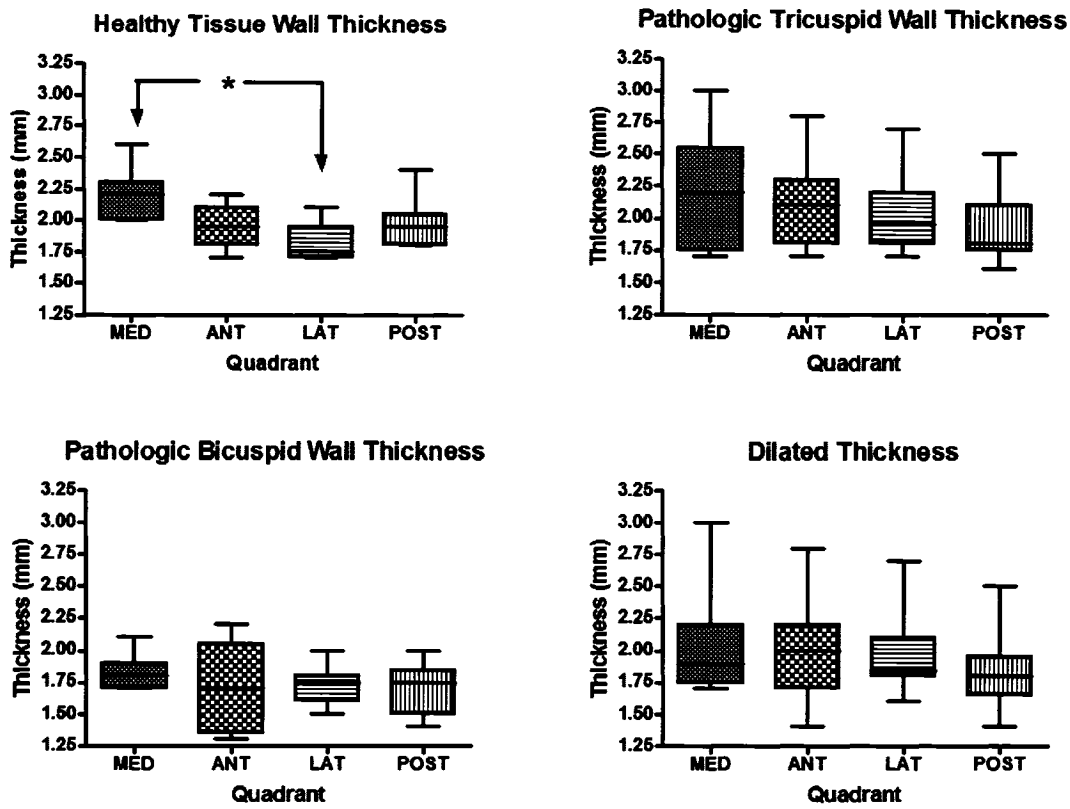

Figure 4.2: Healthy tissue exhibits regional variation in the wall thickness, where tissue from the medial quadrant is thicker than tissue from the lateral quadrant. MED: medial, ANT: anterior, LAT: lateral and POST: posterior quadrants.

4.1.3. Healthy and Pathologic Tissue Comparisons (by aortic valve type)

The data from the previous section was also used for comparison between healthy and pathologic tissue based on valve type. Significant differences were detected for both the thickness variation between quadrants and also between tissue types. Significant regional differences (P=0.0066, two way ANOVA, Bonferroni post test) were detected in both healthy and pathologic tricuspid tissue; pathologic bicuspid tissue did not exhibit any local variation in thickness. The post tests identified that healthy tissue again demonstrated a significant difference between the medial and lateral quadrants and that pathologic tricuspid tissue had different tissue thicknesses between the medial and posterior quadrants. All tissue demonstrated similar circumferential variation with the medial quadrant being the thickest. Also, pathologic bicuspid tissue had the thinnest tissue overall with a P value <0.0001 (two way ANOVA, Figure 4.2).

4.1.4. Healthy and Dilated Tissue Comparisons

Comparisons between healthy and dilated tissue revealed differences in thickness between the quadrants only and not between the types of tissue. Like healthy tissue, there was a significant difference between the quadrants (P=0.0325, two way ANOVA). For healthy tissue the difference was between the medial and lateral quadrants and for dilated tissue between the medial and posterior quadrants (Figure 4.2).

4.2. VARIATION IN MECHANICAL PROPERTIES

Engineering stress-strain curves were used to investigate the circumferential mechanical properties of healthy and pathologic AA tissue. The test, consisting of 13 cycles and a final stretch, lasted 20 minutes. For the duration, data was acquired at a rate of 4 Hz to collect continuous load cell measurements of force and transducer measurements of displacement. Engineering stress-strain curves were generated using the previously discussed equations for stress (σ) and strain (ε) in Section 1.3:

$$\sigma = F / A \tag{1.1}$$

$$\varepsilon = \frac{L - L_o}{L_o} \tag{1.2}$$

where F is the force (N), A is the cross-sectional area (mm^2), L is the deformed tissue length (mm) and L_o (mm) is the initial length. The L value used to determine strain was calculated using the measured displacement (D) and the following equation:

$$L = L_o + D \tag{4.1}$$

These curves provided the engineering stress-strain because the dynamic specimen cross-sectional area was assumed constant. The unloaded, stress-free cross-sectional area was used and measured (discussed in Section 3.2). The acquired data points were converted to stress and strain and plotted for both the axial and circumferential directions using Microsoft Excel (Figure 4.3). All of the samples produced a repeatable stress-strain curve after preconditioning (Figure 4.4). It was seen that the hysteresis loop of the tissue would decrease and shift to the left after each cycle until it stabilized after approximately 5 cycles.

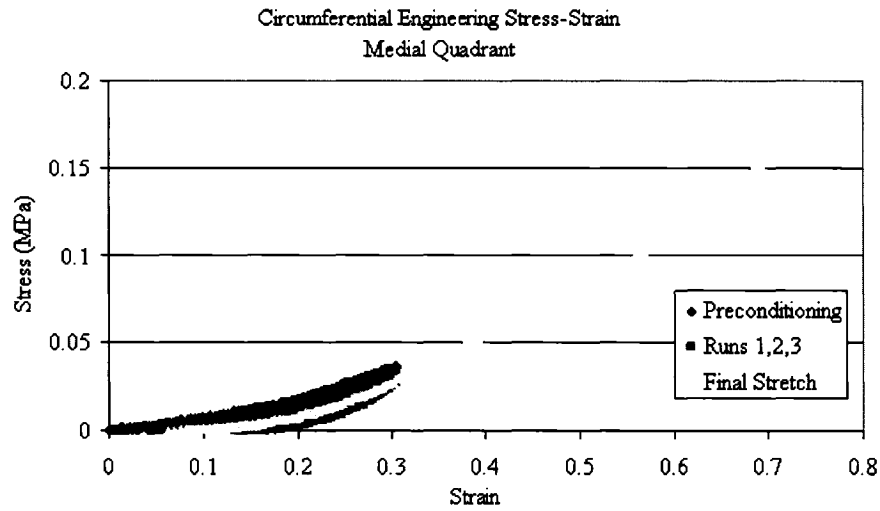

Figure 4.3: Example of the equi-biaxial protocol for the circumferential direction of the medial quadrant of a 58 year old male (sample #2 in Table 3.1). The same graph was also plotted for the axial direction and repeated for each quadrant.

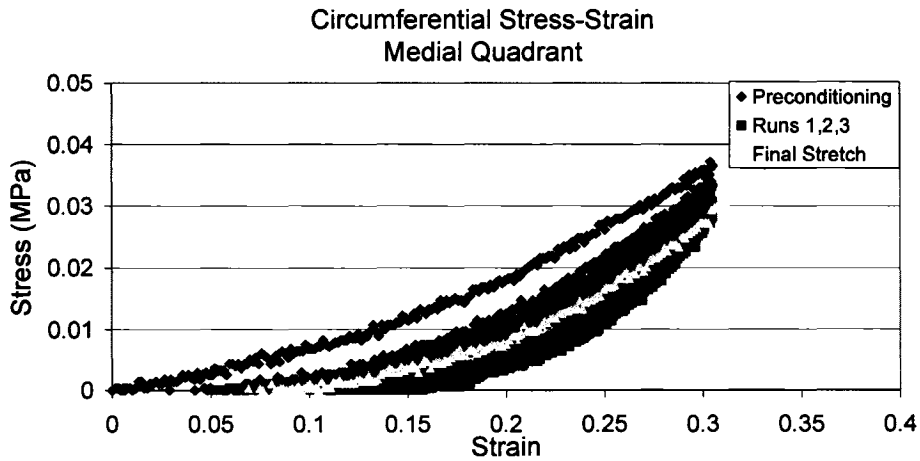

Figure 4.4: The AA tissue response was reproducible after 5 preconditioning cycles and exhibited less hysteresis.

Engineering stress-strain loading curves were also constructed from the data obtained from the final stretch of the tensile test protocol. These curves were generated for each quadrant of tissue and plotted on the same graph for both the circumferential and axial directions (Figure 4.5). This part of the test was designed to bring the tissue to

failure and as a result, the effects of tissue tearing caused for discontinuity in the stress-strain curve at high stresses.

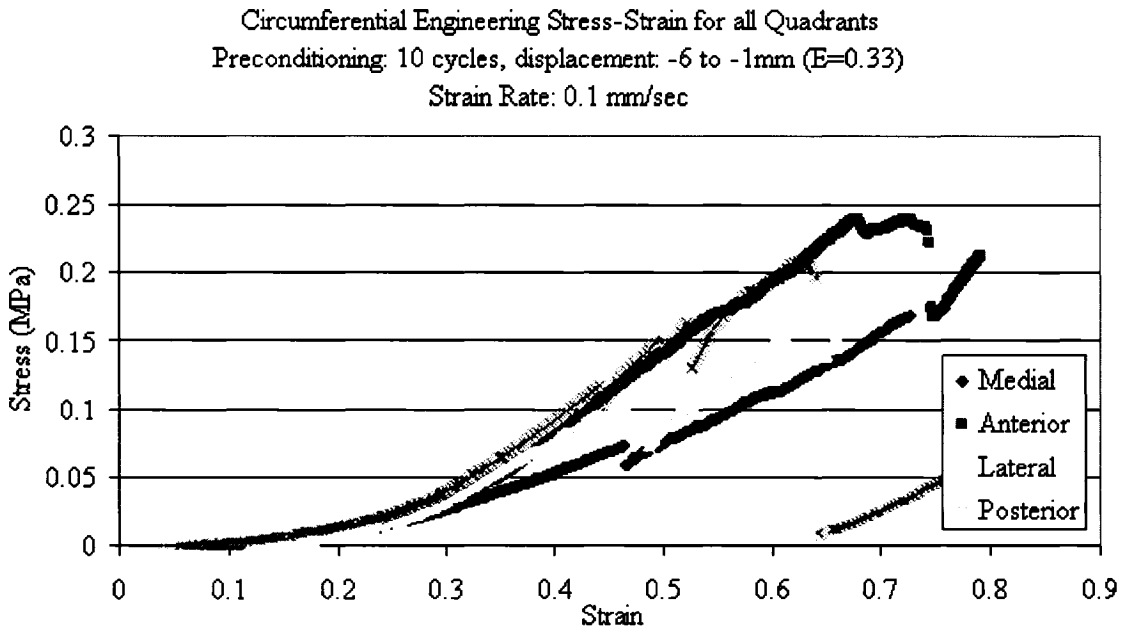

Figure 4.5: Example of stress-strain curves in the circumferential direction obtained from the final stretch for tissue obtained from each quadrant of an aortic ring of a 58 year old male (sample #2 in Table 3.1). The same graph was also plotted for the axial direction. The effect of tissue tearing can be seen in the discontinuity of the curves.

For the statistical analyses comparing the mechanical response of the tissue from each quadrant, elastic moduli were fit to the final stretch stress-strain curves in both the low and high stress regions. As mentioned previously, the low stress elastic moduli (E_e) is associated with the elastin content of the tissue and the strain hardening region elastic moduli (E_{ec}) is related to both the elastin and collagen content of the tissue (Section 1.3.1 and Figure 1.6). These two regions were selected in the loading curve of the tissue; similar to the technique used by Vorp in the investigation of aortic aneurysms [65]. To expose any general trends, the stiffest tissue quadrant and the occurrence and location of failure was also noted for each of the clinical samples tested.

Three types of analyses were conducted. The first lumped all of the tissue together to look into the general population characteristics using one way ANOVA. The second analyzed the characteristics of a given tissue type (healthy, pathologic tricuspid, pathologic bicuspid and dilated) using one way ANOVA. Finally, the tissue types were compared using two way ANOVA. All statistics are presented as mean values ± standard deviation and *P* values <0.05 were considered statistically significant.

4.2.1. All Samples

General statistics were performed to elucidate any trends from the general population (all groups lumped). Column statistics and one way ANOVA were performed to investigate the directional variation of the elastic moduli for the quadrants of the tissue. The mean values along with the standard deviation amongst the tissue are provided (Table 4.3). There were no statistical differences in either moduli between the axial or circumferential direction when the entire patient population was included. The moduli at high strain had larger variability.

Table 4.3: General population mean elastic moduli ± SD for both the circumferential and axial direction.

	Axial	**Circumferential**
E_e (MPa)	0.10 ± 0.05	0.07 ± 0.04
E_{ec} (MPa)	0.61 ± 0.41	0.49 ± 0.30

4.2.2 Tissue Type

For this analysis, the clinical samples were classified into 4 tissue types: healthy, pathologic tricuspid, pathologic bicuspid and dilated. Column statistics and one way ANOVA were used to identify any existing trends for individual tissue types. There were no statistical differences in either moduli for the axial or circumferential direction when the subcategories were included. The mean values and the standard deviation are provided (Table 4.4):

Table 4.4: General tissue types mean elastic moduli ± SD for both the circumferential (circ.) and axial direction. Path Tri: pathologic tissue from tricuspid aortic valve patients and Path Bi: pathologic tissue from bicuspid aortic valve patients.

		Healthy	**Path Tri**	**Path Bi**	**Dilated**
Axial	E_e (MPa)	0.12 ± 0.07	0.08 ± 0.04	0.10 ± 0.04	0.09 ± 0.05
	E_{ec} (MPa)	0.58 ± 0.31	0.78 ± 0.61	0.49 ± 0.17	0.67 ± 0.48
Circ.	E_e (MPa)	0.09 ± 0.04	0.05 ± 0.02	0.08 ± 0.03	0.06 ± 0.03
	E_{ec} (MPa)	0.46 ± 0.23	0.53 ± 0.36	0.48 ± 0.29	0.54 ± 0.34

It can be seen that there exists a high degree of variation in both the low and high stress moduli for all tissue types. The large standard deviation values in both the axial and circumferential directions demonstrate substantial biological variability in the response of the tissue.

4.2.3. Healthy and Pathologic Tissue Comparisons (by aortic valve type)

As statistical differences in the circumferential variation of the mechanical response were not detected in any of these categories of tissue alone, comparisons between the types were conducted. In this analysis, the pathologic tissue was separated

according to patient aortic valve type to test the hypothesis that hemodynamics play a factor in local tissue remodeling of the AA.

All three groups were compared using a two way ANOVA test to investigate differences in the response due to quadrant position and tissue type. The low stress and high stress moduli comparisons for the circumferential direction are provided in Figures 4.6 and 4.7 respectively. Bonferroni's multiple comparisons post tests were used to identify which quadrant was different and/or which tissue type was different.

Statistical differences in the circumferential low stress slope (E_e) were observed (Figure 4.6). The differences were detected for both the circumferential position and tissue type with respective *P* values of 0.0319 and 0.0047 (two way ANOVA). Although the Bonferroni tests could not detect where the differences occurred, it was observed that the pathologic tissue from tricuspid patients had, on average, the lowest slope values. In addition, all three groups demonstrated similar circumferential variation, with the medial and anterior quadrants have the smallest slope values.

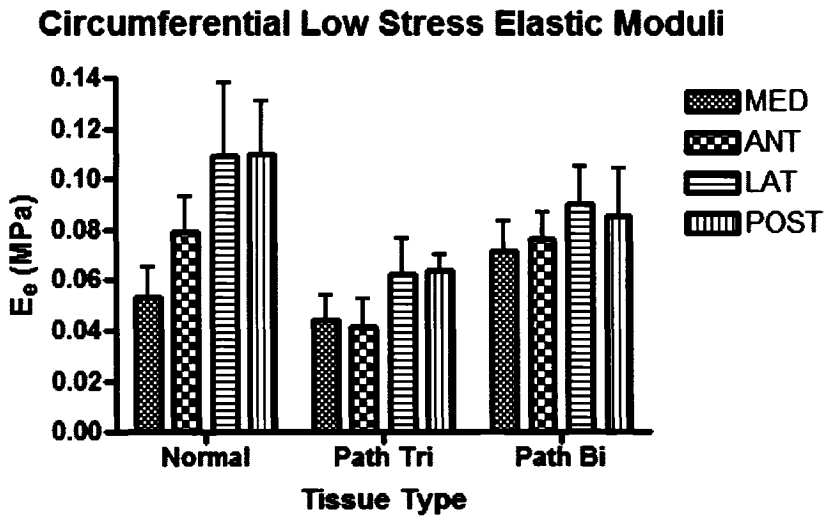

Figure 4.6: Circumferential low stress slope (E_e) comparison in healthy, pathologic tissue from bicuspid and tricuspid aortic valve patient tissue. The moduli varied for different circumferential positions and tissue type.

Though not statistically significant, a similar quadrant variation was noted in the circumferential high stress moduli, where the medial and anterior quadrants values are smaller than the others (Figure 4.7). In addition, it appears that the posterior quadrant becomes stiffer in pathologic tricuspid tissue, when compared to healthy. In contrast to the observations in the low stress response, the average moduli for the pathologic tricuspid tissue are higher than that of healthy tissue. Healthy and pathologic bicuspid tissue moduli are comparable in the high stress region.

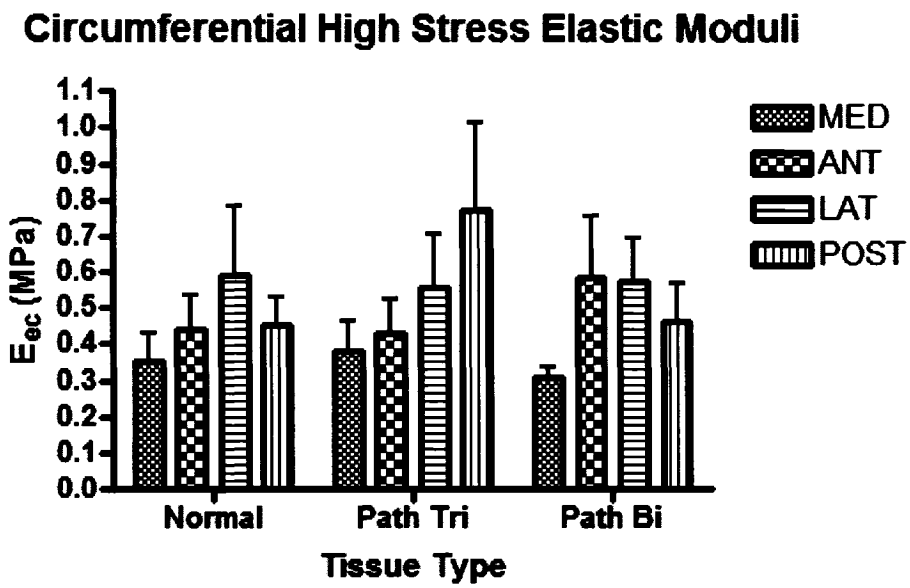

Figure 4.7: Circumferential high stress slope (E_e) comparison in healthy, pathologic tissue from bicuspid and tricuspid aortic valve patient tissue. There were no statistical differences detected.

It can be seen that in healthy tissue, there appears to be a significant difference between the medial quadrant and both the lateral and posterior quadrants in the low stress moduli. The same was noted for the pathological bicuspid tissue in the high stress moduli for the medial quadrant between both the anterior and lateral quadrants. However, a statistical difference was not obtained, most likely due to the small numbers tested.

Comparisons between the groups for the moduli in the axial direction did not show any significant differences (Figures 4.8). Again, this was most likely due to the small number of samples tested. However, the posterior quadrant in healthy tissue appears to be less stiff in both the low and high stress regions. On average, healthy tissue had the highest low stress moduli. In the high stress region, pathologic tricuspid tissue demonstrates large variability in the quadrant moduli.

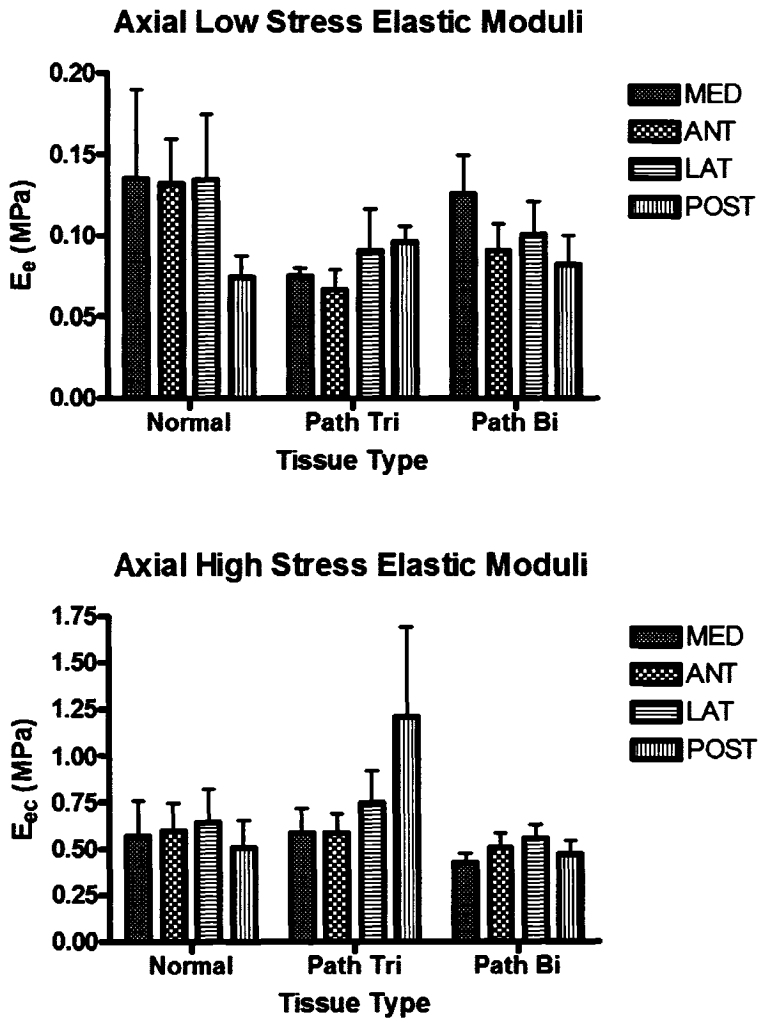

Figure 4.8: Axial low stress slope (E_e) and high stress slope (E_{ec}) comparisons. Low stress axial slope values are higher in healthy tissue than in pathologic tissue. Pathologic tricuspid tissue demonstrates variability in the high stress axial slopes.

4.2.4. Healthy and Dilated Tissue Comparisons

Statistical differences in the circumferential variation were not detected in either healthy or dilated tissue alone; therefore comparisons between the two types were conducted. The groups were compared using two way ANOVA test to investigate differences in the moduli in the circumferential and axial directions between the quadrant and also between the different tissue type. Bonferroni's multiple comparisons post tests were used to identify where this difference occurred.

A statistical difference was detected in the circumferential low stress slope (E_e) for both in the comparisons of quadrants and between the tissue types with respective *P* values of 0.0266 and 0.0248 (two way ANOVA, Figure 4.9). Although the post tests could not identify the location of the differences, it was observed that the medial and anterior quadrants had lower moduli values for both types of tissue. Furthermore, for all quadrants except for the medial, healthy tissue had higher slope values compared to dilated tissue in the low stress region. However, in the high stress region, the slopes for the dilated tissue are higher on average, with the posterior quadrant being the most stiff (Figure 4.10).

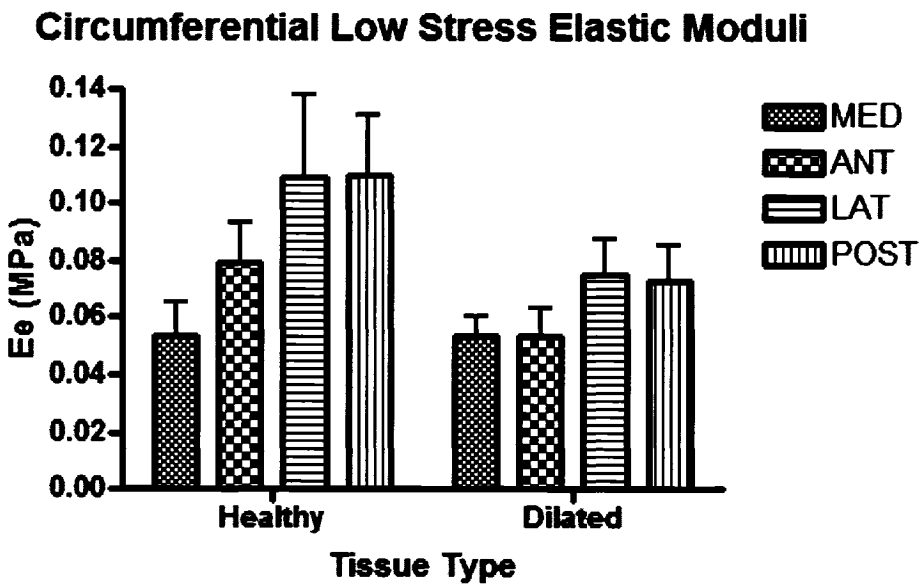

Figure 4.9: Circumferential low stress slope (E_e) comparison of healthy and dilated tissue. Healthy tissue moduli are higher than those of dilated tissue and the medial and anterior quadrants are less stiff than the lateral and posterior quadrants.

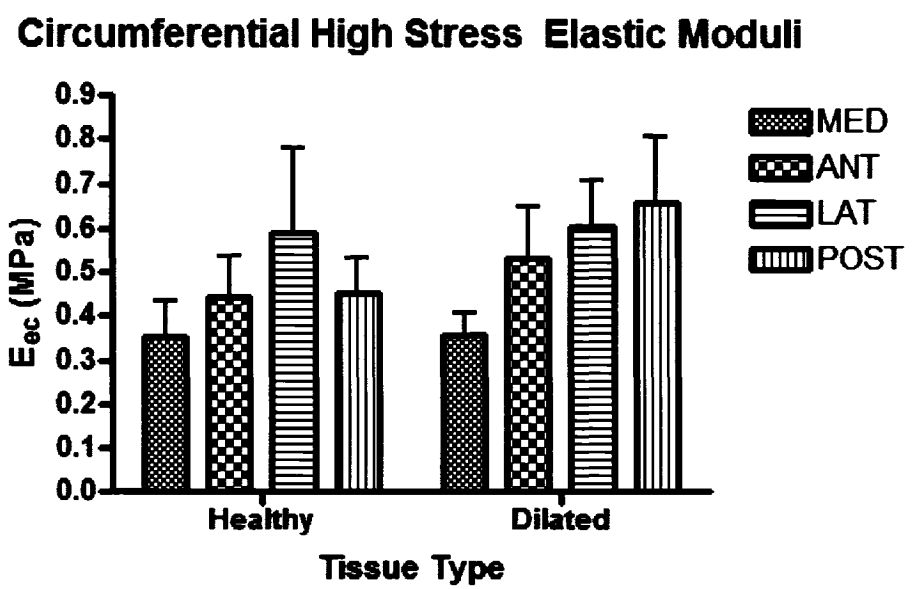

Figure 4.10: Circumferential high stress slope (E_{ec}) comparison of healthy and dilated tissue. No significant differences were detected.

In the axial direction, the quadrant variation in the dilated tissue and healthy tissue slopes values were not evident (Figure 4.11). The axial moduli variation for the healthy tissue has been described in the previous section. For the dilated tissue, there does not appear to be any variation present amongst the quadrants. This may be due to the fact that in this analysis all of the dilated tissue was grouped together, regardless of the valve type present. In the previous analysis, differences between tissues with different aortic valve types were noticed. Therefore, the differences may have been obscured.

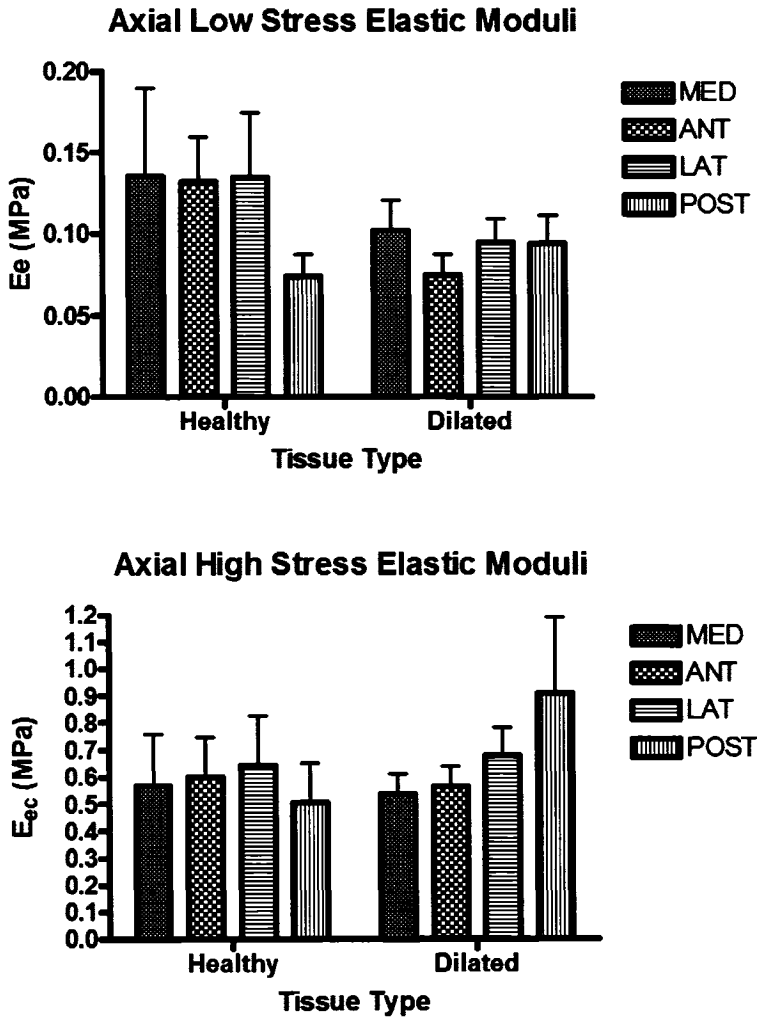

Figure 4.11: Axial low stress (E_e) and high stress (E_{ec}) slope comparisons between healthy and dilated tissue. The moduli between both types of tissue are comparable. No significant differences were detected.

4.3. GENERAL TRENDS

The stiffest tissue quadrant in the high stress region (highest E_{ec}) was noted for both the axial and circumferential directions and failure (axial) of any of the samples during the test were noted to expose any general trends in the tissue. The analysis was first carried out for all tissue and then also for the different types of tissue.

4.3.1. Trends in all Tissue

The results of the stiffest quadrant and occurrence of failure are summarized in Tables 4.5 and 4.6. Circumferentially, the medial quadrant was the stiffest in only one sample (healthy). Furthermore, it was this quadrant that most often failed during the tests. These findings indicate that tissue from the medial quadrant is likely to be the most elastic and least strong as well (Table 4.6).

Table 4.5: The circumferentially stiffest tissue observations for quadrants of all tissue.

	Quadrant			
	Med	**Ant**	**Lat**	**Post**
Stiffest	**1**	**4**	**4**	**6**

Table 4.6: The axially stiffest tissue and occurrence of failure observations for quadrants of all tissue.

	Quadrant			
	Med	**Ant**	**Lat**	**Post**
Stiffest	3	5	5	3
Failure Occurence	12	9	4	4

4.3.2. Trends for Tissue Type

The stiffest tissue quadrant was plotted for the identification of trends in both the circumferential and axial directions per tissue type (Figure 4.12 and 4.13). Statistics were not conducted as this data is non-parametric. In the circumferential direction, it was observed that in pathological tissue, the medial quadrant was never the stiffest, whereas in healthy tissue, the stiffest tissue quadrants were evenly spread out. In pathologic bicuspid and dilated tissue, the posterior quadrants were most likely to be the stiffest. In the axial direction comparisons, the stiffest tissue quadrant was the medial for healthy tissue, posterior for healthy dilated tissue and lateral for pathologic bicuspid tissue.

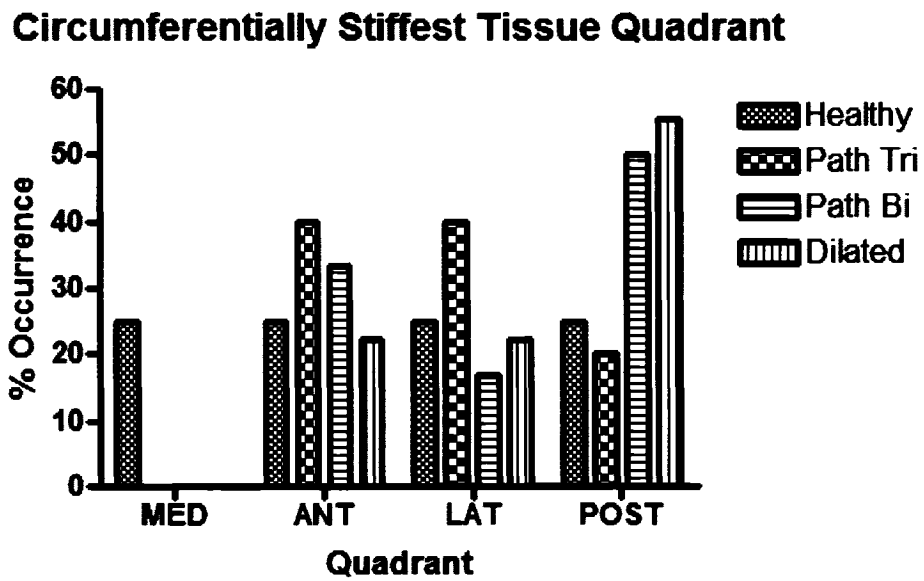

Figure 4.12: Circumferentially stiffest tissue quadrants in healthy, pathologic tricuspid and bicuspid aortic valve patients and dilated tissue.

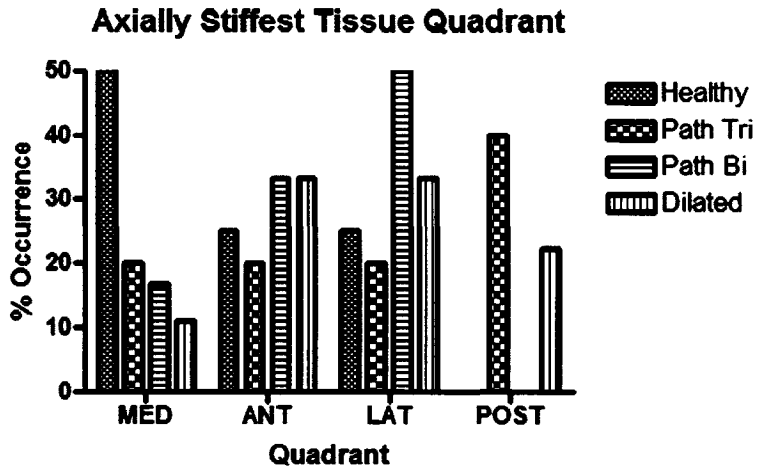

Figure 4.13: Axially stiffest tissue quadrants in healthy, pathologic tricuspid and bicuspid aortic valve patients and dilated tissue.

The occurrence of failure of the tissue during the final stretch of the tissue in the tensile test protocol is summarized in Figure 4.14. Again statistics were not conducted. It was observed that in healthy tissue, the anterior quadrant failed every time. In addition, it was observed that regardless of the tissue type, failure generally occurred most often in the medial quadrant.

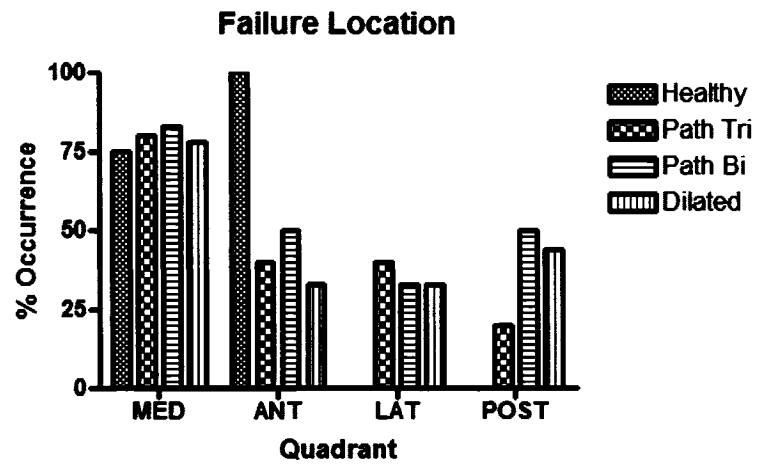

Figure 4.14: Axial failure occurrence in healthy, pathologic tricuspid and bicuspid aortic valve patients and dilated tissue.

4.4. BIAXIAL PROPERTIES AND ASSUMPTIONS USED

For the investigation of the anisotropic biaxial properties of the AA tissue, the non-homogeneous deformation of the tissue had to be taken into account. The data for the displacement transducer was obtained from an equi-biaxial protocol, thus assuming an equal deformation in both the circumferential and axial directions. Therefore, for these analyses a video extensometer was used. The device monitors the actual displacement of the specimen by tracking 4 dots painted as a central square marker of 3 mm x 3 mm on the tissue. As the specimen was stretched, the extensometer outputs the deformation as E_{11}, E_{22} and E_{12} which correspond to the circumferential, axial and shear Green's strains respectively. With the assumption that the shear strain is negligible, the two dimensional Green's strain (E_{ij}) for the circumferential (i=1, j=1) and axial (i=2, j=2) direction is respectively defined as follows:

$$E_{11} = \frac{1}{2}\left(\lambda_{11}^2 - 1\right) \tag{4.2}$$

$$E_{22} = \frac{1}{2}\left(\lambda_{22}^2 - 1\right) \tag{4.3}$$

where λ_{11} and λ_{22} are the extension ratios defined as the ratio of the deformed and original dimensions of the tissue sample along the appropriate axis.

Conventionally, Cauchy stresses are plotted with Green's strain (Figure 4.15). Cauchy stresses (σ_{ii}) differ from engineering stresses because they incorporate the dynamic cross-section of the tissue.

$$\sigma_{ij} = \frac{F_{ij}}{TL_{ij}} \tag{4.4}$$

where F_{ij} is the force along the axes, T is the dynamic thickness, L_{ij} is the dynamic length of the specimen perpendicular to the force applied. With the assumption that the tissue is incompressible, the dynamic thickness was defined in terms of the extension ratios:

$$T = \frac{1}{\lambda_{11}\lambda_{22}} T_0 \tag{4.5}$$

By substituting equation 4.5 into equation 4.4, the Cauchy stresses were calculated:

$$\sigma_{11} = \lambda_{11} \frac{F_{11}}{T_o L_{11o}} \tag{4.6}$$

$$\sigma_{22} = \lambda_{22} \frac{F_{22}}{T_o L_{22o}} \tag{4.7}$$

where λ_{ij} is the extension ratio, F_{ij} is the measured force, T_0 is the undeformed thickness of the tissue and L_{ijo} is the undeformed length measured prior to testing as described in Section 3.2

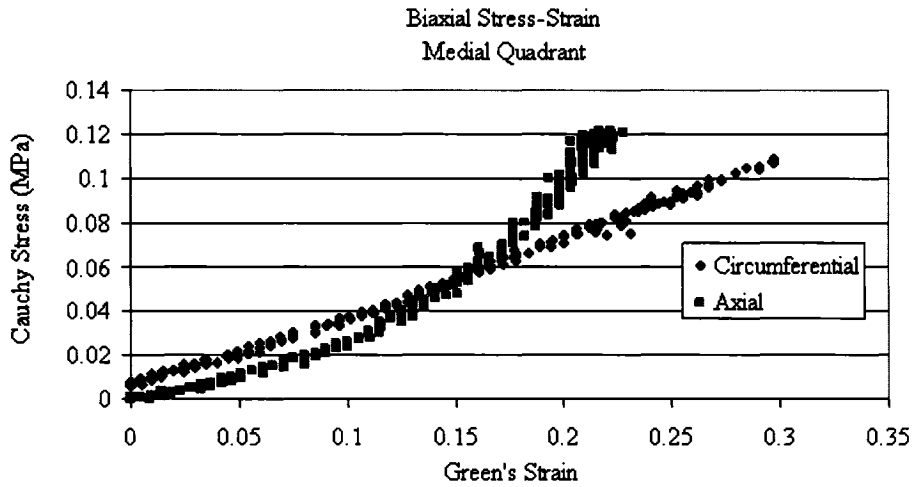

Figure 4.15: Example of Cauchy stress vs. Green's strain curve for the biaxial response from loading after preconditioning of AA tissue from the medial quadrant of a 58 year old male (sample #2 from Table 3.1).

4.4.1. Biaxial Behaviour

To characterize the biaxial behaviour of the AA tissue, the biaxial plots (for each quadrant) of Cauchy stress vs. Green's strain were used. In addition, the direction of failure (if it occurred) was noted. However, the optical extensometer data used in the formulation of these graphs was noisy. Furthermore, in some instances, the tissue would extend past the camera view leading incomplete data sets from the final loading stretch. As a result, only the low stress moduli and the onset of a non-linear (strain hardening) response in the stress-strain curve was used to characterize the anisotropic behaviour of the AA. Finally, the India ink used as a central marker had bled during some of the tests performed; the data from these tests were not included in the analysis. Due to the loss of data from some of the clinical samples, the pathologic tissue data was grouped together (n=8, samples #2, 5, 6, 8, 11, 12, 14 and 15 in Table 3.1), regardless of the type of aortic disease present and the healthy tissue (n=3, samples #1, 3 and 4 from Table 3.1) was not statistically analyzed. The biaxial response and circumferential variation were compared using two way ANOVA. As there were no differences found between the quadrants, the mean values obtained from column statistics along with the standard deviation are provided (Table 4.7).

Table 4.7: General pathologic population mean Cauchy stress and Green's strain low stress elastic moduli ± SD for both the circumferential and axial direction for all tissue.

	Axial	**Circumferential**
E_e (MPa)	0.15 ± 0.12	0.20 ± 0.17

The biaxial response (E_e axial and circumferential) was not significantly correlated with the circumferential location. However, the biaxial low stress moduli (E_e), were significantly different between the axial and circumferential directions with a P value of 0.0322 (two way ANOVA) and therefore, the tissue had an anisotropic response. The circumferential moduli were higher than those in the axial direction for all quadrants

(Figure 4.16). This finding is interesting when compared to the values obtained in the engineering stress-strain data, summarized in Table 4.2. In the engineering data, where the inhomogeneous deformation was not taken into account, the axial direction was stiffer in the low stress region. This suggests that care must be taken when interpreting engineering stress-strain data.

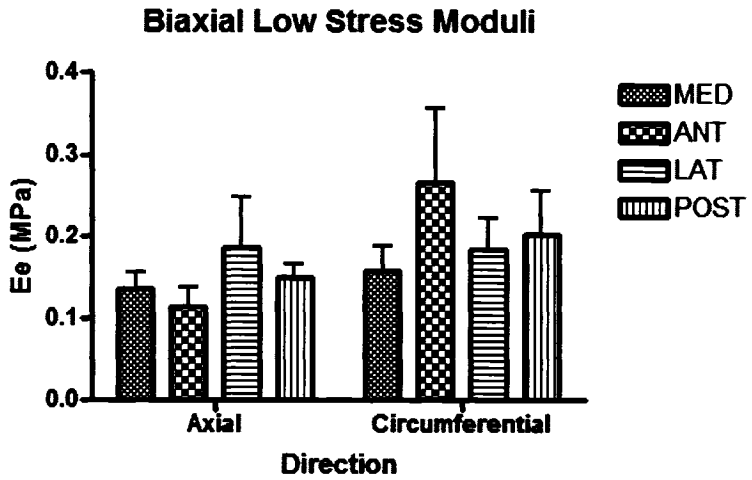

Figure 4.16: Cauchy stress and Green's strain in the biaxial low stress moduli. The moduli in the circumferential direction are significantly higher than in the axial direction for all quadrants.

Past this region, it was noted that if the onset of non-linearity was not isotropic, it was the axial direction that reached this point before the circumferential (this was not true for only 1 case out of 10, anterior quadrant of sample #8 in Table 3.1). This point is further reinforced in the biaxial failure properties. It was noted that the initial tear and eventual failure of the tissue occurred in the axial direction but for a few exceptions (Figure 4.17).

Figure 4.17: Failure of the tissue in the circumferential direction during the final stretch of the tensile test protocol in the axial direction.

5. RESULTS: HISTOLOGICAL ANALYSIS

A total of 37 clinical samples, 7 healthy and 30 pathologic, were used in the histological analysis (Section 3.1). For each sample, 4 Movat pentachrome stained histology slides (one from each quadrant) were obtained. The staining allowed for the different components in the tissue to be distinguished; the components of interest were elastin (black), collagen (yellow) and SMCs (red). Digital microscopy was used to take 9 representative pictures of each slide (3 regions in the radial direction and 3 regions along the circumference). The dimensions of each image (40x magnification) were 0.13 mm x 0.17 mm, with an approximately area of 0.02 mm^2 (Figure 5.1). Nine regions were taken to obtain a adequate representation of the entire slide.

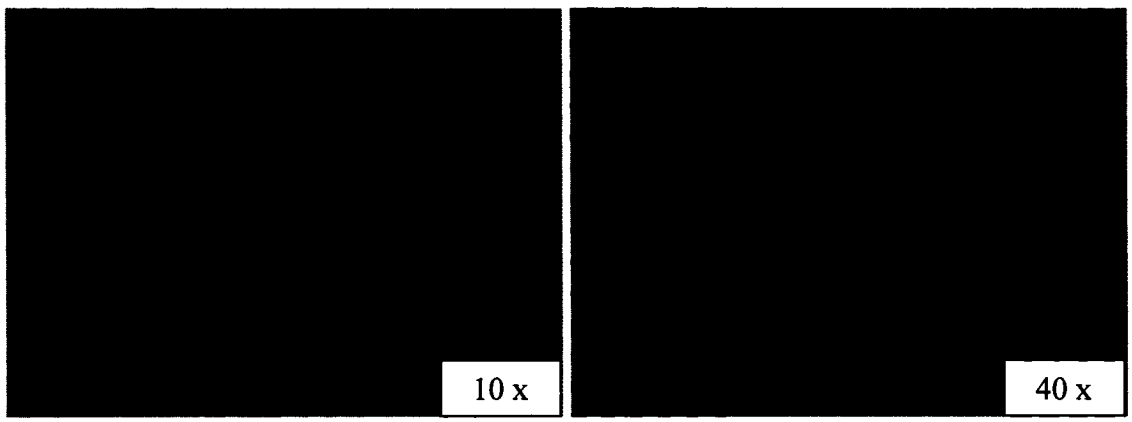

Figure 5.1: Calibration slide used in image analysis. The images are under 10x and 40x magnification respectively. The area of an image magnified 40x is approximately 0.02 mm^2.

A semi-quantization of the tissue composition was obtained using a program written in MATLAB that counted the pixels by colour and divided this number by the total pixels present in the digital image. A total of 27 measurements were made per quadrant (a reading for elastin, collagen and SMCs per image taken from the 9 images per slide). The grouping of clinical samples was the same as the biomechanical analysis. The patient characteristics are provided along with the standard deviation (Table 5.1).

Table 5.1: Patient characteristics for histological analysis. Pathologic tissue was grouped according to aortic valve type (BAV/TAV) and also as dilated for comparisons with healthy tissue. BAV: bicuspid aortic valve and TAV: tricuspid aortic valve.

	Tissue Type			
	Healthy	**Pathologic**		
Patient Characteristics	TAV (n=7)	BAV (n=15)	TAV (n=15)	Dilated (n=16)
Age	61 ± 17	62 ± 16	59 ± 8	63 ± 9
M/F	3/4	14/1	11/4	12/4

5.1. VARIATION IN COMPOSITION

For statistical analyses, the program percentage outputs (pixels for a given colour / total pixels) for elastin, collagen and SMCs were used. As mentioned previously, these are the components that are involved in the passive mechanical response of AA tissue. Unlike the biomechanics section that investigated differences in the axial and circumferential direction, in the histological analysis, it is the variation in tissue composition in the radial and circumferential directions that was investigated.

Three types of analyses were conducted. The first lumped all of the tissue together to look into the general population tissue content characteristics using one way ANOVA. The second analyzed the characteristics of a given tissue type using one way ANOVA. Finally, the tissue types were compared using two way ANOVA. All statistics are presented as mean values ± standard deviation. P values <0.05 were considered statistically significant.

5.1.1. All Samples

General statistics were performed to elucidate any trends from the general population (all groups lumped). Column statistics and one way ANOVA were performed to investigate the directional variation in tissue content. The mean values amongst all tissue for the content of elastin, collagen and SMCs, along with the standard deviation are provided. There were no significant differences in the tissue content detected between the quadrants. Radially, however, a significantly higher SMCs content was detected in the region closest to the adventitia with a *P* value of 0.011 (one way ANOVA, Bonferroni post tests). The post tests identified that the SMCs in the outer region of the media was significantly different from that of both the middle region and the inner region closest to the intima for all types of tissue (Figure 5.1).

Table 5.2: Mean component composition ± SD of the major structural components (all tissue).

	Component		
	Elastin	**Collagen**	**Smooth Muscle Cells**
% Composition	25.5 ± 6.6	11.2 ± 4.2	13.1 ± 4.2

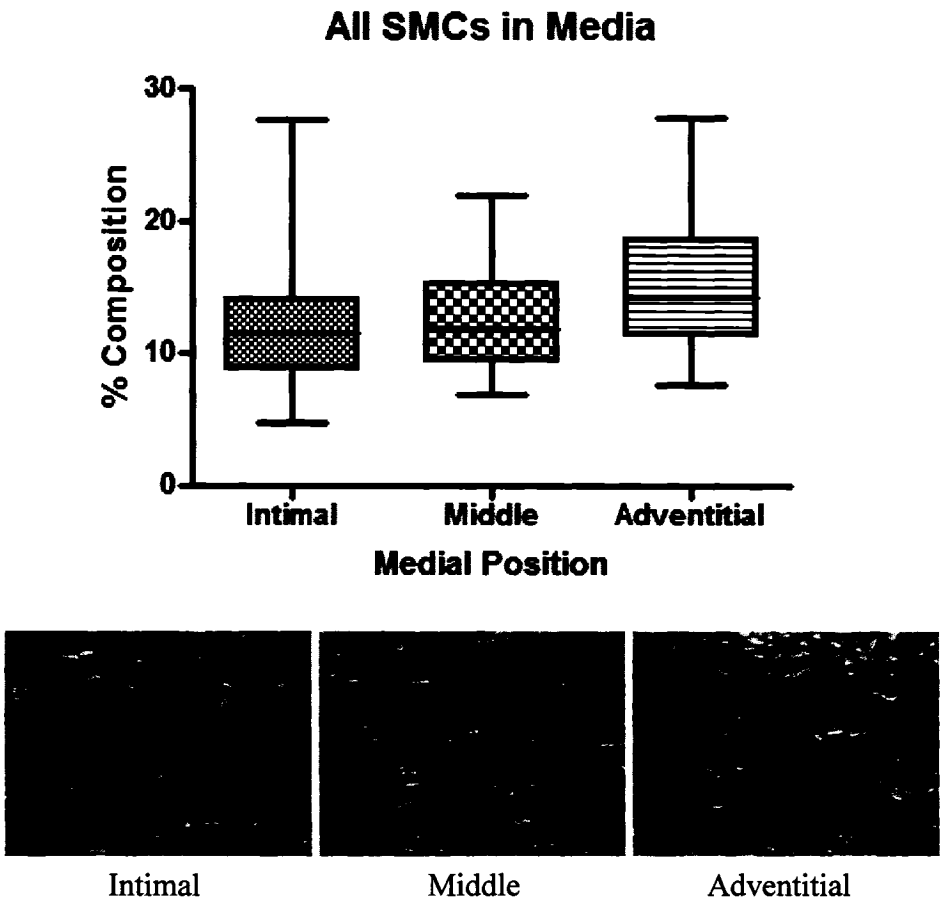

Figure 5.2: Medial SMCs (red) distribution for all tissue types. As can be seen in both the graph and histology pictures, the region closest to the adventitia contains on average more SMCs. In this case, thickening of the elastic plates was also observed in this region.

5.1.2. Tissue Type

For this analysis, the clinical samples were classified into 4 tissue types: healthy, pathologic tricuspid, pathologic bicuspid and dilated. The mean values for the percent composition of the structural components for the different tissue types are provided in Table 5.3.

Table 5.3: General tissue types mean component composition ± SD. Path Tri: pathologic tissue from tricuspid aortic valve patients and Path Bi: pathologic tissue from bicuspid aortic valve patients. For the components, E: elastin, C: collagen and SMCs: smooth muscle cells.

		Healthy	Path Tri	Path Bi	Dilated
% Composition	E	22.9 ± 6.5	27.3 ± 7.2	25.0 ± 5.6	25.9 ± 7.2
	C	9.4 ± 3.1	11.1 ± 5.0	12.1 ± 3.6	10.5 ± 4.1
	SMCs	11.9 ± 3.3	13.0 ± 5.0	13.8 ± 3.7	12.4 ± 3.8
	Other	55.8 ± 6.5	48.7 ± 10.8	49.1 ± 9.0	51.2 ± 10.3

It can be seen that the tissue composition of all of the specimens are comparable. In healthy tissue, however, there is less of every component. This finding suggests that there is a compaction in the medial layer in the diseased samples. Comparisons of tissue thickness in the previous section had established that the bicuspid aortic tissue was thinner than the other types. A compaction of the medial layer is likely related to the loss of mucopolysaccharides. Therefore, a category of the remainder of the components present in the medial layer has been included in the analysis. This category quantifies the amount of mucopolysaccharides, interstitial fluids and fat (void spaces) present in the tissue.

Column statistics and one way ANOVA were used to identify if there was any significant variation in tissue content amongst the quadrants and throughout the medial layer in the radial direction. Again, there were no significant variations of the components between the quadrants. The SMCs content exhibited variation in the media for healthy tissue; more SMCs were detected in the region closest to the adventitia (P=0.0147, one way ANOVA, Bonferroni's post test, Figure 5.3).

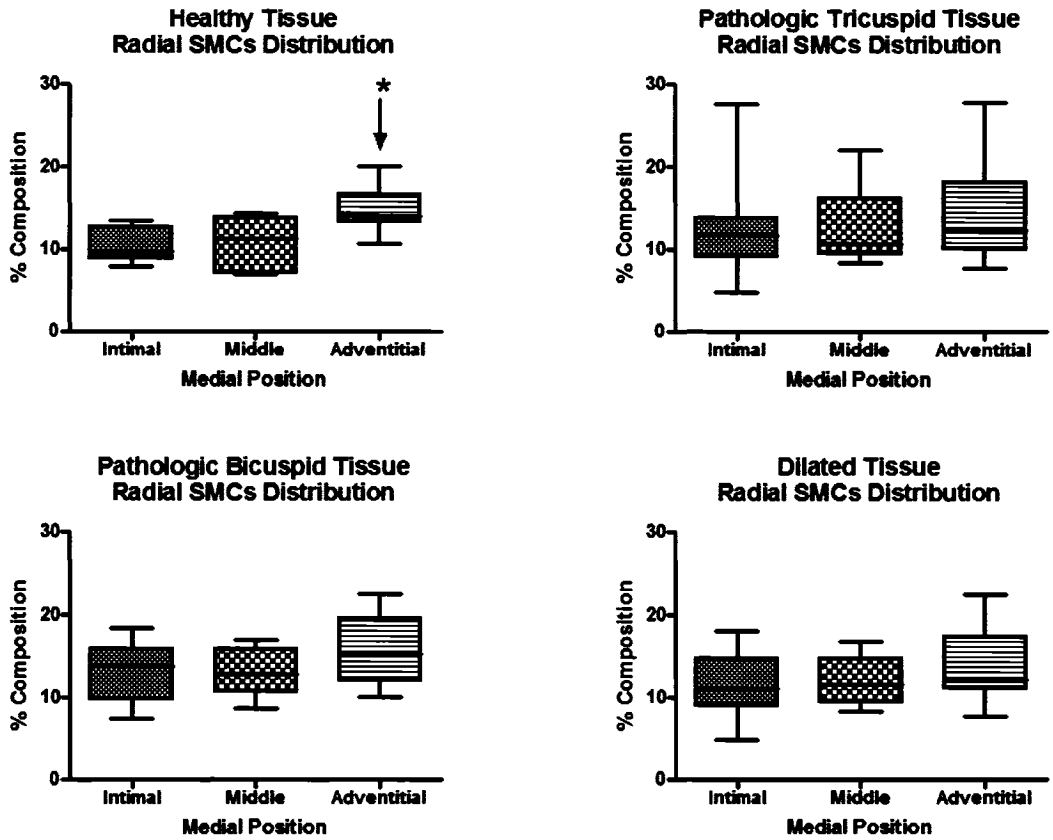

Figure 5.3: Significant radial variation in SMCs content was detected in healthy tissue only. There were more SMCs in the outer region of the media.

All tissue demonstrated variations of the other components content within the media (Figure 5.4). In healthy tissue, there was significantly less of the other components in the region closest to the adventitia than in the middle region (P=0.0177, one way ANOVA, Bonferroni's post test). The pathologic tissue demonstrated an opposite trend; the region closest to the adventitia had a higher content of the other components; each group had a P value <0.001. This finding suggests that medial compaction occurring with disease is concentrated in the region closest to the intima.

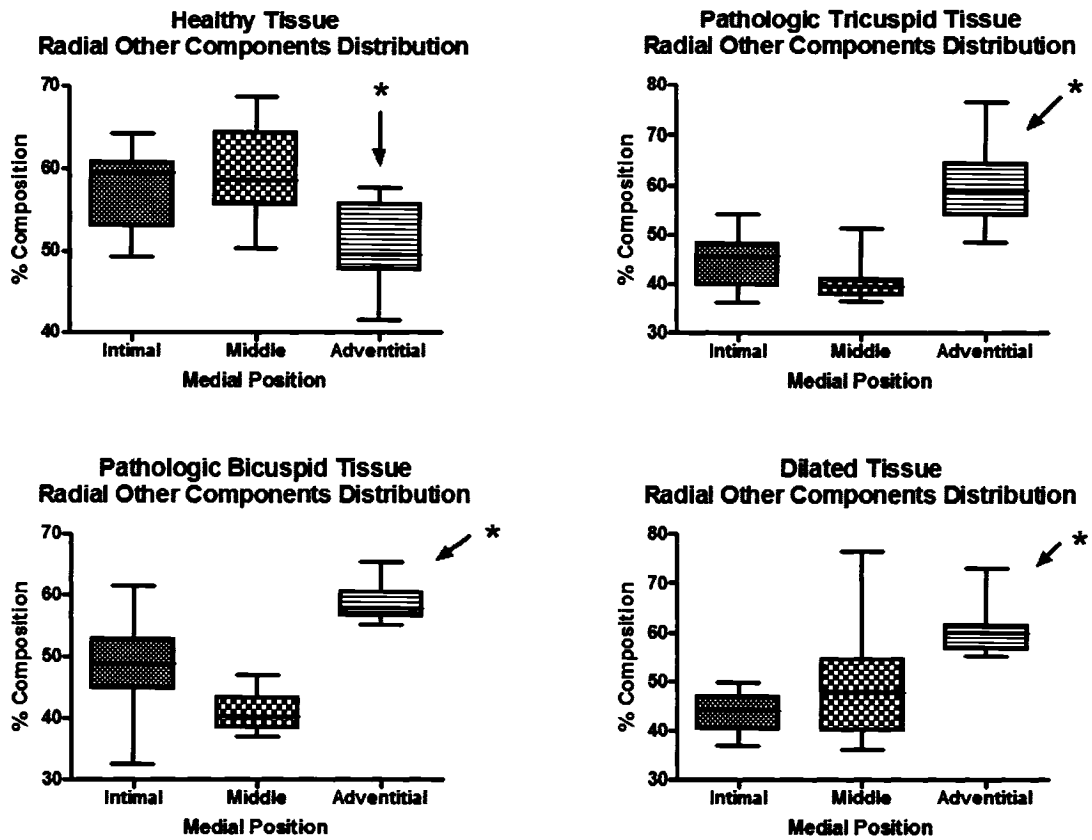

Figure 5.4: All tissue types had significant differences in the medial content of the other components in the radial direction. Healthy tissue demonstrated an opposite variation than pathologic tissue, where the latter had significantly more of the other components in the region closest to the adventitia.

5.1.3. Healthy and Pathologic Tissue Comparisons (by aortic valve type)

Statistical analyses were also conducted to detect differences in tissue composition between healthy and pathologic tissue categorized by valve type. The three groups were compared using a two way ANOVA test to investigate both the local variation and difference between tissue types. Whenever a statistical difference was found between the groups, Bonferroni's multiple comparisons post tests were used to identify where this difference occurred.

There were no significant differences in the content of the tissue between the quadrants. Once again, within the media, there were more SMCs detected in the region of the media closest to the adventitia (P=0.0082, two way ANOVA) and also, a difference in collagen was detected between tissue types (P=0.00255, two way ANOVA, Figure 5.5). Healthy tissue contains a significantly lower percentage of collagen than the pathologic tissue types.

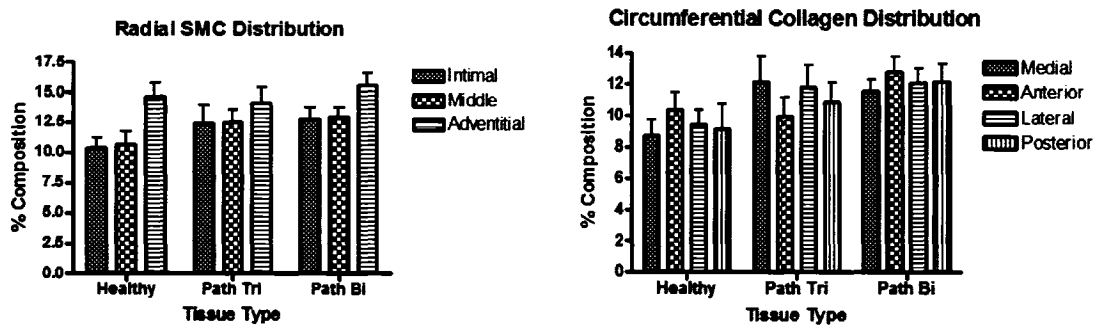

Figure 5.5: Differences were detected for SMCs content within the media and healthy tissue contains significantly less collagen than the pathologic types.

Significant differences were found between tissue types in the elastin content of the tissue as well, in both the radial and circumferential directions (P=0.0334 and P=0.0208 respectively, two way ANOVA, Figure 5.6). Although the post tests could not identify which of the three groups were significantly different, it was noted that the greatest difference was observed between healthy and pathologic tricuspid tissue, with the latter containing a higher percentage of elastin overall. Although it was not significant, it can also be seen that healthy and pathologic tricuspid tissue exhibit regional variation, unlike pathologic bicuspid tissue. The medial quadrant in both healthy and pathologic tricuspid tissue appears to have a higher percentage in elastin content.

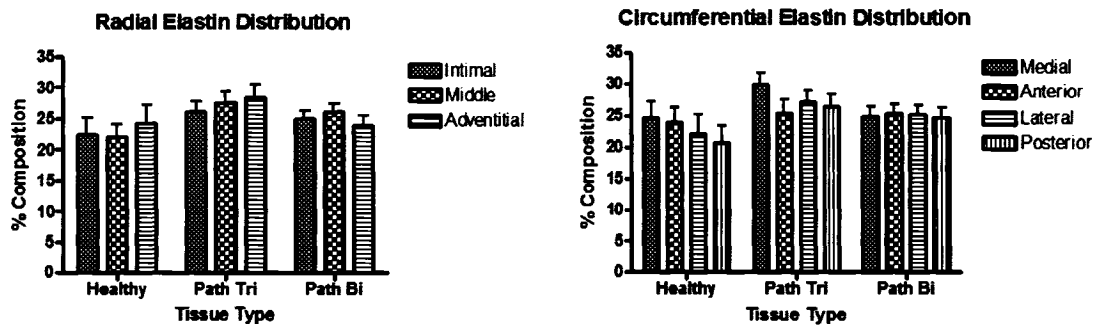

Figure 5.6: Radial and circumferential elastin distribution for all tissue types. A significant difference was detected in the comparison of tissue types.

Significant differences were also detected for the tissue content of the other components (Figure 5.7). In the radial analysis, the differences were found for both the tissue type and medial position ($P<0.001$ both cases, two way ANOVA). In the circumferential analysis, differences were found between the tissue types only ($P=0.0043$, two way ANOVA). Overall, healthy tissue contains more of the other components than the pathologic tissue. The post tests identified that all of the tissue exhibited radial differences between the middle and near adventitial regions; the healthy tissue demonstrates an opposite variation than that of the pathologic tissue.

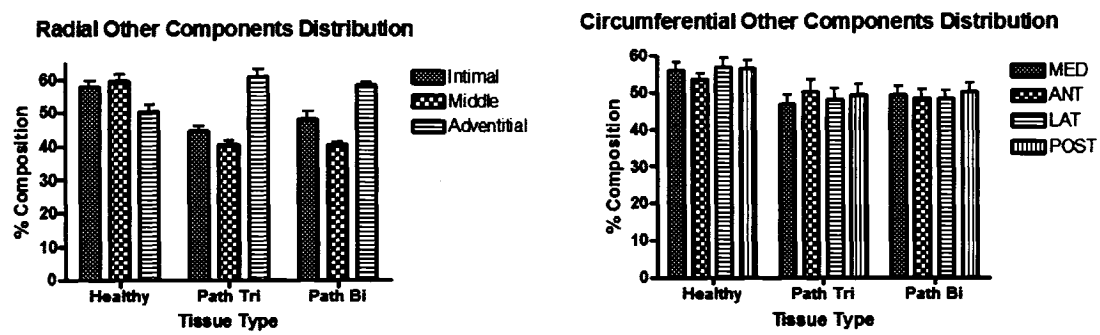

Figure 5.7: Radial and circumferential distribution of other components for the tissue types. Healthy tissue contains more of the other components than healthy tissue. Pathologic bicuspid and tricuspid radial tissue distributions are similar.

5.1.4. Healthy and Dilated Tissue Comparisons

Statistical analyses were also conducted to detect differences in tissue composition between healthy and dilated tissue. The groups were compared using a two way ANOVA test to investigate differences in the response due to location and tissue type. Whenever a statistical difference was found between the groups, Bonferroni's multiple comparisons post tests were used to identify where this difference occurred.

There were no significant differences detected between the quadrants. However, radial differences were significant; the results are summarized in Figure 5.8. As in the preceding analyses, a radial difference with more SMCs present in the region closest to the adventitia was noted (P=0.0116, two way ANOVA). Healthy tissue contained significantly more of the other component content than dilated (P=0.0184, two way ANOVA). Although not significant, it appears that both types of tissue demonstrate radial variation (opposite) in other component content.

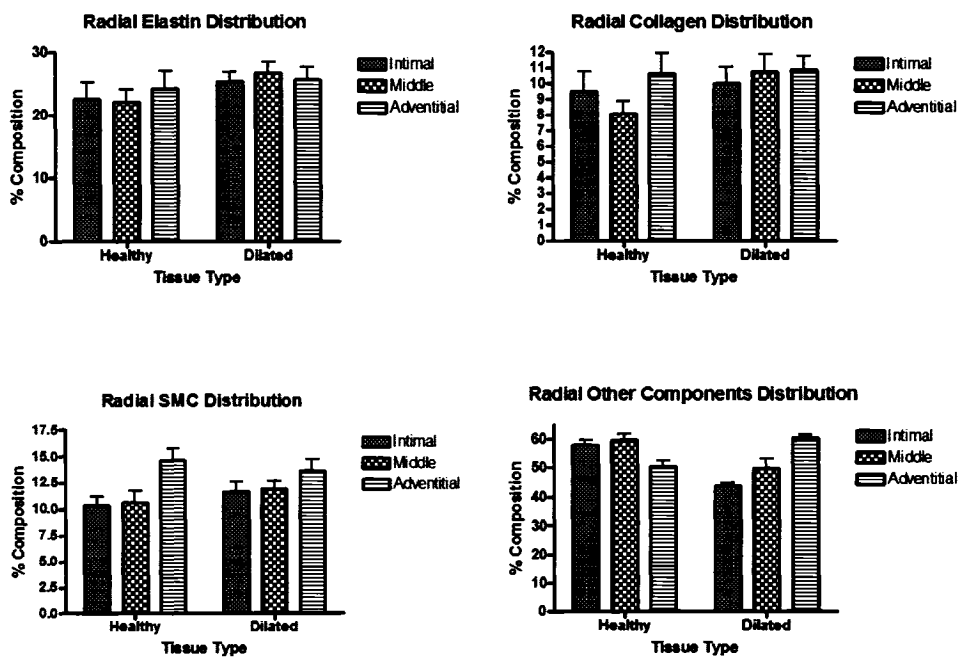

Figure 5.8: Comparisons of components between healthy and dilated tissue. No significant differences were detected.

5.2. GENERAL TRENDS (all tissue)

The occurrence of significant differences in tissue content between the quadrants and throughout the media was also noted for each case. A summary of the results are given for both the radial and circumferential direction (Table 5.4 and Table 5.5) respectively. It was observed that for local variation in the radial direction, the SMCs content was most often significantly different between the regions closest to the intima and the adventitia. In fact, it appears that the region with the highest SMCs content is that closest to the adventitia. For all components, it was found that for almost every case (29 out of 31), the near adventitial region was different. The most significant local variation in components in the circumferential direction was noted most frequently for elastin in the anterior quadrant.

Table 5.4: Local significance in the differences between components in the radial direction. For the components, E: elastin, C: collagen and SMCs: smooth muscle cells. For the regions, Int: intimal, Mid: middle, Adv: adventitial. Most of the significance was detected for SMCs between the region closest to the intima and that closest to the adventitia.

		Region		
Component	**Significant Cases**	**Int-Mid**	**Int-Adv**	**Mid-Adv**
E	9	1	2	6
C	8	2	3	3
SMCs	17	--	10	7

Table 5.5: Local differences between component composition in the circumferential direction. For the components, E: elastin, C: collagen and SMCs: smooth muscle cells. For the quadrants, Med: medial, Ant: anterior, Lat: lateral and Post: posterior. Most of the significance was found for elastin in the anterior quadrant.

		Quadrant			
Component	**Significant Cases**	**Med**	**Ant**	**Lat**	**Post**
E	30	11	18	14	15
C	12	6	9	5	10
SMCs	13	6	10	6	4

6. DISCUSSION

The key finding in this study was that regional differences do exist in human AA tissue, supporting the hypothesis of this study. In tissue thickness comparisons, it was seen that the medial quadrant was the thickest. Mechanically, the medial quadrant was generally the least stiff circumferentially and the most likely to fail. Although histologically, differences in tissue content between the quadrants were not detected, local variation throughout the media was seen. Interestingly, local differences occurred in both healthy and pathologic AA tissue, with the quadrant variation least evident in pathologic bicuspid tissue. This finding suggests that circumferential variation in tissue properties are aortic valve dependent, that tissue remodeling is related to the hemodynamics in the AA. Since BAVs can have any leaflet orientation; it seems likely that classifying all pathologic bicuspid tissue together would not demonstrate significant local variation in tissue properties.

This thesis investigated the retrospective tissue histology and *in vitro* passive tissue mechanics. The histological analysis was semi-quantitative and only accounted for the three major structural components. A consistent protocol was used for all biomechanical testing. However due to the viscoelastic nature of vascular tissue, it was difficult to relate our findings to other studies; the results are dependent on the preconditioning protocols and strain rates used.

Past studies have linked the biomechanical response of vascular tissue to its structural components. The low stress response of the tissue is related to the stretching of elastic fibres within the tissue and is thus related to the elastin content. At high stresses exceeding the physiological range, the response of the tissue is attributed to collagen fibres uncoiling. The SMCs contribute to the active response of the tissue; however, it has been observed that they do not contribute significantly to the passive mechanical response of large blood vessels such as the aorta [13].

Many risk factors are likely to increase the prevalence of vascular diseases, such as family history, hypertension, obesity, smoking and dietary fat content. However, none of these factors account for the focal nature of the diseases. It is widely accepted that hemodynamic forces cause local tissue remodeling leading to focal disease formation. No study to date has evaluated the focal nature of human AA tissue remodeling. This phenomenon has been investigated in this work. The results from this study have been divided into two categories: 1) healthy vs. pathologic tissue based on aortic valve type and 2) healthy vs. dilated tissue.

The first analysis was conducted to investigate whether local tissue variations occur. If hemodynamics are involved in the development and progression of disease, local tissue remodeling should be evident. The flow in the AA is highly dependent on the aortic valve leaflets and thus the presence of a BAV would result in altered blood flow patterns in the aorta than that with an aorta with a TAV.

The second analysis stems from the fact that all pathologies lead to weakening of the media that eventually results in dilatation of the blood vessel. It has been shown that an increase in lumen diameter of a blood vessel increases the stresses it incurs. As a result, the higher circumferential stresses associated with dilatation may be a significant factor in the development of pathologies.

6.1. MAJOR FINDINGS IN STUDIES OF ALL TISSUE

The results from the measurements of tissue thickness amongst the quadrants revealed that tissue from the medial quadrant was significantly thicker (Figure 4.1). In the mechanical tests, it was the medial quadrant that was most likely to fail and also the least likely to be the stiffest (Tables 4.5 and 4.6). Also, a discrepancy between the local moduli obtained from engineering and Cauchy stress-Green's strain stress-strain curves was observed. The engineering curves indicated that the axial direction was stiffer than the circumferential, whereas in the Cauchy stress-Green's strain curves, the opposite was

true. This discrepancy may be attributed to the fact that in the latter case, the dynamic cross-sectional area was taken into account.

The histological analysis had identified that in all tissue, regardless of whether it is healthy or diseased, regional variation in tissue content within the media exists (Figure 5.2). SMCs had a significantly higher percent composition in the region closest to the adventitia. Local variations were observed between the quadrants only when the analyses were patient specific (no lumping of tissue samples). This suggests a large variation in tissue content between different samples. In the histological analysis of individual tissue samples, it was observed that the anterior quadrant tends to be significantly different in its elastin content (Table 5.5).

Interestingly, the overall trends from the analyses have indicated that although the medial quadrant was less stiff and thicker, this tissue was also most likely to fail (Table 4.14). This finding suggests that the medial quadrant has a tissue composition that leads to it being a weaker material than that of the other quadrants. Although not significant, in healthy and pathologic tricuspid tissue, the medial quadrant appeared to have a higher percentage of elastin content than the others. The structure and organization of the components in the medial quadrant may also be attributed to this finding. During the histological analysis, focal alterations were noted in the elastic plates, such as the breaking of the elastic lamellae. In some instances, the plates appeared to be thicker, most likely due to the fusion of adjacent plates occurring with the loss of SMCs.

The average composition of tissue was compared for the different tissue types: healthy, pathologic tricuspid, pathologic bicuspid and dilated. Although no significant differences were found, it appeared that healthy tissue contained significantly smaller percent composition of elastin, collagen and SMCs than pathologic tissue (Table 5.3). This contradicts past work that has cited that the pathologic media contains less of these components. This finding suggests the compaction of the medial layer (involved with medial degeneration) in pathologic tissue.

6.2. MAJOR FINDINGS IN STUDIES BASED ON VALVE TYPE

The findings from the biomechanical and histological analyses for comparisons of samples with pathological tissue classified according to aortic valve type were summarized. The findings were further discussed to identify any associations present between the mechanical response and composition of the tissue.

6.2.1. Tissue Type Variation

The results from the biomechanical analyses in the present study have found that AA tissue from BAV patients is significantly stiffer than tissue from TAV patients in the low stress region (Figure 4.6). This trend can be attributed to the fact that the average wall thickness of pathologic bicuspid tissue was thinner than the other types of tissue (Figure 4.2). Comparisons between the groups of tissue in the high stress moduli (associated with collagen content) in both directions revealed that the slopes were generally comparable as no significant differences were detected.

The histology results from comparisons of healthy and pathologic tissue based on valve type detected a significant difference in the elastin content. Although the post tests did not identify where the difference occurred; it was noted that pathologic bicuspid tissue contained less elastin than pathologic tricuspid tissue (Figure 5.6). Also, the pathologic bicuspid tissue had a higher percentage of collagen content than pathologic tricuspid tissue (Figure 5.5). This finding suggests that different forms of medial degeneration between pathologic tricuspid and pathologic bicuspid tissue may be present.

Work done by Bechtel *et al.* has indicated that pathologic AAs with a BAV have less severe aortic wall abnormalities than those with TAV despite a similar degree of aortic dilatation [11]. This includes less elastic plate fragmentation, medial necrosis, atherosclerosis and fibrosis (grading according to histological standard criteria [66]). Their results suggest that the pathology associated with BAV thus cannot be detected by light

microscopy criteria and that there may be different mechanisms involved in AA dilatation with BAV. Their work, however, was qualitative; they did not quantify the amount of structural components present. In this study, however, a semi-quantitative approach was used and has been successful in identifying the differences between the types of tissue.

Parai *et al.* have found significant differences in elastin content between AAs in patients with BAV and TAV using morphometry [67]. They have concluded that pathologic bicuspid tissue contains less elastin than pathologic tricuspid tissue, consistent with the results from this work. Past work by Nistri *et al.* had found that the aorta in BAV patients is stiffer and less distensible in the high stress region than in TAV patients, which agrees with the results that pathologic bicuspid tissue contains more collagen [68]. Interestingly, in our study, pathologic bicuspid tissue stiffness did not differ significantly from pathologic tricuspid tissue in the axial direction.

6.2.2. Regional Variation

The analyses have also identified significant regional variation. The results from this study have shown that the medial and anterior quadrants are thicker than the lateral and posterior quadrants (Figure 4.2). Significant differences between the thicknesses of the quadrants were detected for healthy tissue between the medial and lateral quadrants and for pathologic tricuspid tissue between the medial and posterior quadrants. No significant variation was found for the pathologic bicuspid tissue. Mechanically, the medial quadrant is generally less stiff circumferentially regardless of the tissue type in both the low and high stress regions (Figures 4.6 and 4.7). Overall, the mechanical variation between quadrants was most apparent in healthy tissue and least obvious in pathologic bicuspid tissue. This circumferential variation reflects the circumferential thickness variation in the tissue as thickness inversely dictates the amount of stress a material experiences. Nicosia *et al.* compared tissue from the anterior and posterior quadrants of porcine aortic root tissue using biaxial tensile tests [69]. Overall, they found tissue from the anterior region to be biaxially more extensible than that from the posterior

region. However, it is important to note that the porcine aortic valve morphology is different from human, with the valve consisting of two large cusps and one small cusp. This difference would most likely contribute to a different hemodynamic profile than that in humans.

Histologically, there were no differences in tissue content detected between quadrants. However radially, there were was a higher percentage of SMCs content in the medial region closest to the adventitia for all types of tissue (Figure 5.5).

6.3. MAJOR FINDINGS IN STUDIES BASED ON AA DILATATION

The findings from the histological and biomechanical analyses for comparisons of samples with pathological tissue classified according to aortic diameter (Ø < 50 mm for dilated tissue). The findings were further discussed to identify any associations present between the composition and mechanical response of the tissue.

6.3.1. Tissue Type Variation

There were less significant differences found in this analysis than in the preceding section, most likely due to lumping samples from different aortic valve types together. The analyses from the mechanics identified that the circumferential low stress moduli were significantly lower in dilated tissue than in healthy (Figure 4.2). Okamoto *et al.* [70] have also found similar results; when they compared their data on the ultimate strength of dilated tissue to that of normal tissue by Mohan and Melvin, the strength of dilated tissue was lower [71]. Similarly, Vorp *et al.* have found that aneurysmal AAs have lower local slope values (similar to the ones used in this study) than healthy tissue, although they did not detect any significant differences [65]. Their values are in the same order of magnitude as those obtained in this study (Table 6.1). The difference in the values is most likely due to the different preconditioning protocols and strain rates used.

Table 6.1: Comparison of low stress moduli of healthy and dilated tissue compared to values found in literature [65].

		Healthy	Dilated
Axial	E_e (MPa)	0.12 ± 0.07	0.09 ± 0.05
	Vorp: E_e (MPa)	0.45 ± 0.16	0.42 ± 0.05

6.3.2. Regional Variation

In the thickness analyses, the medial quadrant was found to be significantly thicker than the lateral quadrant in healthy tissue and thicker than the posterior quadrant in dilated tissue (Figure 4.2). Furthermore, circumferential variation was also detected from the mechanics, the medial and anterior quadrants were less stiff than the lateral and posterior quadrants for both types of tissue (Figures 4.9 and 4.10).

The histological analysis did not detect any significant differences in tissue content between the quadrants. However, once again a local variation in the radial direction was identified; there were more SMCs in the region of the media closest to the adventitia. No other significant trend was detected in the regional composition of the major structural components.

6.4. MAJOR FINDINGS IN STUDIES IN AA BIAXIAL RESPONSE

Cauchy stress was plotted against Green's strain for the investigation of the biaxial tissue response. These stresses and strains were used because they incorporate the inhomogeneous, real time deformation of the tissue during the tensile test. Many difficulties were experienced in using the optical strain extensometer and as a result, some of the data was lost or excluded from the analysis. Due to the limited data, only the low stress moduli were compared and all of the pathological specimens were grouped together.

As was previously described, the data obtained using the optical strain extensometer and that from the load cells and displacement transducers (used in the formulation of the engineering stress-strain curves) yielded different results. In the engineering stress-strain curves, the axial low stress moduli were found to be higher than the circumferential, whereas in the Cauchy stress vs. Green's strain moduli, the opposite was true. This finding suggests that care must be taken in the interpretation of engineering stress-strain curves. They may not reflect the true mechanical properties of an anisotropic material. This was not a problem in this study; the data from the engineering stress-strain curves was used comparatively.

Some studies have investigated the equi-biaxial response of human aortic tissue using real time measurements of tissue deformation. Vande Geest *et al.* studied the biomechanical behaviour of human infrarenal aortic tissue under equi-biaxial tension control [72]. They noted that the peak stretch was not significantly different when the axial and circumferential directions were compared. Mohan and Melvin also did not find any significant differences in the ultimate stress values between the two directions in descending mid-thoracic human aorta [57]. They did, however, note that in equi-biaxial stretch tests, the tissue always failed due to stretching in the axial direction, a phenomenon that has also been noted in this study. Okamoto *et al.* have found that in dilated human AA tissue, the equi-biaxial stress-stretch results indicated that the tissue was somewhat anisotropic, but did not find a consistent direction of anisotropy [70]. In the present study, comparison of the mean moduli values for all tissue demonstrated that the circumferential direction was stiffer than the axial overall. However, the results from the individual cases also did not find a consistent direction of anisotropy.

6.5. LIMITATIONS

The limitations of this study require some attention as there are many difficulties that arise with the testing of biological materials. The aorta is a viscoelastic, anisotropic

and heterogeneous material. These properties had to be accounted for during testing and in the analysis of this study.

The foremost limitation was the specimen size. Healthy AA has a diameter of approximately 2-3 cm. This study required tissue from each quadrant of an aortic ring and as such, the maximum specimen size that could be used was 1.5 x 1.5 cm. Larger specimen sizes would have been preferable so that the effect of the sutures on the central region (monitored by the optical strain extensometer) could be kept to a minimum.

As described previously, a viscoelastic material demonstrates hysteresis, creep and stress relaxation. To account for these properties, the AA tissue was preconditioned until the hysteresis loop stabilized (to account for relaxation and creep) and was significantly smaller than at the start. However, the loading and unloading curves still were not coincident and thus only the loading curve was used in the study and the unloading curve ignored. Viscoelastic materials also exhibit a strain history dependence and therefore, a given tissue sample could not be tested more than once.

The anisotropic mechanical properties of the tissue resulted in inhomogeneous deformation and distortion at the suture points. The deformation was monitored optically to counter this. However, the use of the optical strain extensometer resulted in further difficulties. Often the ink used as markers would bleed and result in the loss of data. Furthermore, the method was extremely sensitive to light. The intimal surface of the tissue was shiny and therefore the presence of light would make it difficult for the optical extensometer to track the markers with high resolution.

The heterogeneous nature of the tissue caused for difficulty in identifying the material axes. Furthermore, in the mechanical analysis, it was assumed that the tissue was radially homogeneous. As such, the contribution of the adventitial layer was ignored. Also there was large specimen to specimen variability both within a clinical sample and between different samples. This was most evident in the histological analysis. Although many replicates were taken for a given microscope slide, there was

still a high standard deviation in the results. If a larger number of clinical samples were used, more significant differences in the analyses would likely have been detected. Furthermore, the staining of the slides was not consistent; the images had varying colour intensities. Although, the MATLAB program could compensate for the variance; it was often difficult to quantify the collagen pixels (which varied from light yellow to dark orange in colour).

Finally, the tensile tests were carried out *in vitro*. Care was taken to reproduce physiological conditions, such as the use of biaxial tests and floating the tissue in physiological saline to prevent it from drying out. However, the tests were carried out at room temperature. At room temperature, the SMCs contribution to the biomechanical response is diminished. Also the reference state used was one of zero load and zero strain. Physiologically, arterial tissue is in a loaded state due to blood pressure and once they are removed from the body, the tissue retracts axially. Furthermore, once the tissue is excised from the body, it starts to degrade; limiting the testing time available. All tissue was stored in saline solution at 4 °C and tested within 48 hours; however although not significant, some biological degradation would have taken place.

7. CONCLUSIONS

In summary, this work has reported the mechanical and structural properties of human AA tissue obtained from autopsy and excised surgical tissue. This is the first study to show that local differences in tissue properties exist in both healthy and pathologic human AA.

Circumferential variability was observed in the tissue mechanics. Overall, the medial quadrant was the thickest, least stiff and most likely to fail. Histologically it was observed that this quadrant appeared to contain more elastin. Statistical differences were most evident when the pathological tissue samples were classified according to the aortic valve type (BAV/TAV). Comparisons between the patient groups revealed that healthy and pathologic tricuspid tissue exhibit similar variations in tissue content, thickness and mechanical response between the quadrants, whereas in pathologic bicuspid tissue, the differences were less pronounced or non existent. This suggests that the valve type influences the tissue remodeling in the AA, most likely due to hemodynamic differences.

Although variations in tissue content were not evident in the four quadrants, significant radial variations were detected in the histological analysis. It was seen that all tissue types contained a higher percentage of SMCs in the region of the media closest to the adventitia. It was also noted that all tissue demonstrated regional variability in the mucopolysacharrides, interstitial fluid and fat category. Healthy tissue had a higher SMCs content in the region closest to the adventitia; a trend opposite to that in pathologic tissue. This finding suggests that that the medial compaction associated with disease occurs locally in the region closest to the intima.

The results from this study indicate that regional differences are present in both healthy and diseased human AA tissue, indicating that the assumption of homogeneity in tissue properties may not be a valid one. Furthermore, it appears that biomechanical properties vary in accordance with the structural components in the media; predominantly with elastin and mucopolysaccharides. The information obtained is invaluable for

computational modeling of the left ventricle outflow tract to predict wall stresses in the AA, the design of prosthetic devices and provides fundamental insights to the pathobiology of aortic diseases.

8. RECOMMENDATIONS

Some recommendations are provided for those wishing to pursue future studies on the mechanical and structural properties of the AA. The foremost subject is that this study investigated *in vitro* passive tissue mechanics. Although the tissue was tested within 48 hours of excision from the body or harvesting from autopsy, some degradation is likely to have occurred. To better simulate the physiological response of the tissue, active tests that chemically stimulate SMCs conducted at body temperature (37 °C) with sinusoidal loading (similar to systolic and diastolic pressure involved with the heart beating) is recommended. Furthermore, the histological analysis was semi-quantitative. A biochemical quantization of the structural components may prove to have less variation and be able to detect more significant local variations in tissue content. Such a method was developed in this study using high pressure liquid chromatography (HPLC) to quantify the amount of hydroxyproline (a secondary amino acid common to both elastin and collagen) present in the tissue. Finally, more AA samples should be tested to overcome the large biological variability that is present between tissues from different patients.

9. REFERENCES

1. Heart Disease: A Textbook of Cardiovascular Medicine. 2001. Saunders.

2. Gozna ER, Marble AE, Shaw AJ, Winter DA. Mechanical properties of the ascending thoracic aorta of man. *Cardiovasc Res.* 1973;7:261-265.

3. Silver FH, Christiansen DL, Buntin CM. Mechanical properties of the aorta: a review. *Crit Rev Biomed Eng.* 1989;17:323-358.

4. Tortora GJ. Principles of Human Anotomy. 2002. John Wiley & Sons, New York.

5. Shadwick RE. Mechanical design in arteries. *J Exp Biol.* 1999;202 Pt 23:3305-3313.

6. Fung YC. Biomechanics: mechanical porperties of living tissues. 1993. Springer-Verlag, New York.

7. Levick JR. An introduction to cardiovascular physiology. 2000. Oxford University Press, New York.

8. Lawrence R, Hartmann DJ, Sonenshein GE. Transforming growth factor beta 1 stimulates type V collagen expression in bovine vascular smooth muscle cells. *J Biol Chem.* 1994;269:9603-9609.

9. Butany J, Ahluwalia MS, Leask RL, Silverside C, Graba J, Williams WG. Pulmonary site porcine bioprosthesis: evaluation at 14 years. *Can J Cardiol.* 2002;18:1173-1175.

10. Lakhani SR, Dilly SA, Finlayson CJ. Basic Pathology. 1998. Oxford University Press, New York.

11. Matthias Bechtel JF, Noack F, Sayk F, Erasmi AW, Bartels C, Sievers HH. Histopathological grading of ascending aortic aneurysm: comparison of patients with bicuspid versus tricuspid aortic valve. *J Heart Valve Dis.* 2003;12:54-59.

12. Kouchoukos NT, Dougenis D. Surgery of the thoracic aorta. *N Engl J Med.* 1997;336:1876-1888.

13. Thompson RW, Geraghty PJ, Lee JK. Abdominal aortic aneurysms: basic mechanisms and clinical implications. *Curr Probl Surg.* 2002;39:110-230.

14. Feizi O, Farrer BG, Emanuel R. Familial study of hypertrophic cardiomyopathy and congenital aortic valve disease. *Am J Cardiol.* 1978;41:956-964.

15. Nataatmadja M, West M, West J, Summers K, Walker P, Nagata M, Watanabe T. Abnormal extracellular matrix protein transport associated with increased apoptosis of vascular smooth muscle cells in marfan syndrome and bicuspid aortic valve thoracic aortic aneurysm. *Circ.* 2003;108 Suppl 1:II329-II334.

16. Fedak PW, de Sa MP, Verma S, Nili N, Kazemian P, Butany J, Strauss BH, Weisel RD, David TE. Vascular matrix remodeling in patients with bicuspid aortic valve malformations: implications for aortic dilatation. *J Thorac Cardiovasc Surg.* 2003;126:797-806.

17. American Heart Association. Heart disease and stroke statistics-2004 update. 2003. Dallas, Tex, American Heart Association.
Ref Type: Report

18. Hashimoto A, Kitamura N, Koyanagi H, Konno S. Surgical treatment of annulo-aortic ectasia. *J Cardiovasc Surg (Torino).* 1976;17:240-247.

19. Grey DP, Ott DA, Cooley DA. Surgical treatment of aneurysm of the ascending aorta with aortic insufficiency. A selective approach. *J Thorac Cardiovasc Surg.* 1983;86:864-877.

20. Morishita K, Abe T, Fukada J, Sato H, Shiiku C. A surgical method for selecting appropriate size of graft in aortic root remodeling. *Ann Thorac Surg.* 1998;65:1795-1796.

21. David TE. Reoperations on the aortic valve combined with replacement of the ascending aorta. *J Card Surg.* 2002;17:46-50.

22. David TE. Aortic valve sparing operations. *Ann Thorac Surg.* 2002;73:1029-1030.

23. David TE, Ivanov J, Armstrong S, Feindel CM, Webb GD. Aortic valve-sparing operations in patients with aneurysms of the aortic root or ascending aorta. *Ann Thorac Surg.* 2002;74:S1758-S1761.

24. Yacoub MH, Gehle P, Chandrasekaran V, Birks EJ, Child A, Radley-Smith R. Late results of a valve-preserving operation in patients with aneurysms of the ascending aorta and root. *J Thorac Cardiovasc Surg.* 1998;115:1080-1090.

25. Nichols WW, O'Rourke MF. McDonald's blood flow in arteries. 1990. Lea & Febiger, Philadelphia.

26. Stergiopulos N, Segers P, Westerhof N. Use of pulse pressure method for estimating total arterial compliance in vivo. *Am J Physiol.* 1999;276:H424-H428.

27. Arteaga-Solis E, Gayraud B, Ramirez F. Elastic and collagenous networks in vascular diseases. *Cell Struct Funct.* 2000;25:69-72.

28. Halme T, Savunen T, Aho H, Vihersaari T, Penttinen R. Elastin and collagen in the aortic wall: changes in the Marfan syndrome and annuloaortic ectasia. *Exp Mol Pathol.* 1985;43:1-12.

29. Pasierski TJ, Binkley PF, Pearson AC. Evaluation of aortic distensibility with transesophageal echocardiography. *Am Heart J.* 1992;123:1288-1292.

30. Vulliemoz S, Stergiopulos N, Meuli R. Estimation of local aortic elastic properties with MRI. *Magn Reson Med.* 2002;47:649-654.

31. Raghavan ML, Webster MW, Vorp DA. Ex vivo biomechanical behavior of abdominal aortic aneurysm: assessment using a new mathematical model. *Ann Biomed Eng.* 1996;24:573-582.

32. Manufacturing with Materials. 1990. The Open University, Oxford.

33. Berry CL, Greenwald SE, Rivett JF. Static mechanical properties of the developing and mature rat aorta. *Cardiovasc Res.* 1975;9:669-678.

34. Halloran BG, Davis VA, McManus BM, Lynch TG, Baxter BT. Localization of aortic disease is associated with intrinsic differences in aortic structure. *J Surg Res.* 1995;59:17-22.

35. Patel DJ, Janicki JS, Carew TE. Static anisotropic elastic properties of the aorta in living dogs. *Circ Res.* 1969;25:765-779.

36. Bauer RD, Busse R, Schabert A. Mechanical properties of arteries. *Biorheology.* 1982;19:409-424.

37. Callister WD. Materials science and engineering: an introduction. 2000. John Wiley & Sons, Inc., New York.

38. Langewouters GJ, Wesseling KH, Goedhard WJ. The static elastic properties of 45 human thoracic and 20 abdominal aortas in vitro and the parameters of a new model. *J Biomech.* 1984;17:425-435.

39. Carew TE, Vaishnav RN, Patel DJ. Compressibility of the arterial wall. *Circ Res.* 1968;23:61-68.

40. Tickner EG, Sacks AH. A theory for the static elastic behavior of blood vessels. *Biorheology.* 1967;4:151-168.

41. Fung YC, Fronek K, Patitucci P. Pseudoelasticity of arteries and the choice of its mathematical expression. *Am J Physiol.* 1979;237:H620-H631.

42. Hayashi K. Experimental approaches on measuring the mechanical properties and constitutive laws of arterial walls. *J Biomech Eng.* 1993;115:481-488.

43. Mirsky I. Ventricular and arterial wall stresses based on large deformation analyses. *Biophys J.* 1973;13:1141-1159.

44. Vito R. A note on arterial elasticity. *J Biomech.* 1973;6:561-564.

45. Vito RP, Hickey J. The mechanical properties of soft tissues--II: the elastic response of arterial segments. *J Biomech.* 1980;13:951-957.

46. Humphrey JD. Cardiovascular Solid Mechanics. 2002. Springer, New York.

47. Simon BR, Kobayashi AS, Strandness DE, Wiederhielm CA. Reevaluation of arterial constitutive relations. A finite-deformation approach. *Circ Res.* 1972;30:491-500.

48. Vaishnav RN, Young JT, Patel DJ. Distribution of stresses and of strain-energy density through the wall thickness in a canine aortic segment. *Circ Res.* 1973;32:577-583.

49. Hudetz AG, Monos E. Characterization of anisotropic elastic properties of the arteries by exponential and polynomial strain energy functions. *Acta Physiol Acad Sci Hung.* 1981;57:111-122.

50. Humphrey JD. Cardiovascular Solid Mechanics. 2002. Springer, New York.

51. von Maltzahn WW, Warriyar RG, Keitzer WF. Experimental measurements of elastic properties of media and adventitia of bovine carotid arteries. *J Biomech.* 1984;17:839-847.

52. Holzapfel GA, Gasser TC, Ogden RW. A New Constitutive Framework for Arterial Wall Mechanics and a Comparative Study of Material Models. *J Elasticity.* 2000;61:1-48.

53. Zulliger MA, Fridez P, Hayashi K, Stergiopulos N. A strain energy function for arteries accounting for wall composition and structure. *J Biomech.* 2004;37:989-1000.

54. Zhou J, Fung YC. The degree of nonlinearity and anisotropy of blood vessel elasticity. *Proc Natl Acad Sci U S A.* 1997;94:14255-14260.

55. Matsumoto T, Abe H, Ohashi T, Kato Y, Sato M. Local elastic modulus of atherosclerotic lesions of rabbit thoracic aortas measured by pipette aspiration method. *Physiol Meas.* 2002;23:635-648.

56. Mohan D, Melvin JW. Failure properties of passive human aortic tissue. I--uniaxial tension tests. *J Biomech.* 1982;15:887-902.

57. Mohan D, Melvin JW. Failure properties of passive human aortic tissue. II--Biaxial tension tests. *J Biomech.* 1983;16:31-44.

58. Thubrikar MJ, Labrosse M, Robicsek F, Al Soudi J, Fowler B. Mechanical properties of abdominal aortic aneurysm wall. *J Med Eng Technol.* 2001;25:133-142.

59. Agozzino L, Ferraraccio F, Esposito S, Trocciola A, Parente A, Della CA, De Feo M, Cotrufo M. Medial degeneration does not involve uniformly the whole ascending aorta: morphological, biochemical and clinical correlations. *Eur J Cardiothorac Surg.* 2002;21:675-682.

60. Vorp DA, Raghavan ML, Webster MW. Mechanical wall stress in abdominal aortic aneurysm: influence of diameter and asymmetry. *J Vasc Surg.* 1998;27:632-639.

61. Ishii T, Asuwa N. Collagen and elastin degradation by matrix metalloproteinases and tissue inhibitors of matrix metalloproteinase in aortic dissection. *Hum Pathol.* 2000;31:640-646.

62. Matsumoto S, Kobayashi T, Katoh M, Saito S, Ikeda Y, Kobori M, Masuho Y, Watanabe T. Expression and localization of matrix metalloproteinase-12 in the aorta of cholesterol-fed rabbits: relationship to lesion development. *Am J Pathol.* 1998;153:109-119.

63. Angouras D, Sokolis DP, Dosios T, Kostomitsopoulos N, Boudoulas H, Skalkeas G, Karayannacos PE. Effect of impaired vasa vasorum flow on the structure and mechanics of the thoracic aorta: implications for the pathogenesis of aortic dissection. *Eur J Cardiothorac Surg.* 2000;17:468-473.

64. Garvey W, Fathi A, Bigelow F, Carpenter B, Jimenez C. Improved Movat pentachrome stain. *Stain Technol.* 1986;61:60-62.

65. Vorp DA, Schiro BJ, Ehrlich MP, Juvonen TS, Ergin MA, Griffith BP. Effect of aneurysm on the tensile strength and biomechanical behavior of the ascending thoracic aorta. *Ann Thorac Surg.* 2003;75:1210-1214.

66. Klima T, Spjut HJ, Coelho A, Gray AG, Wukasch DC, Reul GJ, Jr., Cooley DA. The morphology of ascending aortic aneurysms. *Hum Pathol.* 1983;14:810-817.

67. Parai JL, Masters RG, Walley VM, Stinson WA, Veinot JP. Aortic medial changes associated with bicuspid aortic valve: myth or reality? *Can J Cardiol.* 1999;15:1233-1238.

68. Nistri S, Sorbo MD, Basso C, Thiene G. Bicuspid aortic valve: abnormal aortic elastic properties. *J Heart Valve Dis.* 2002;11:369-373.

69. Nicosia MA, Kasalko JS, Cochran RP, Einstein DR, Kunzelman KS. Biaxial mechanical properties of porcine ascending aortic wall tissue. *J Heart Valve Dis.* 2002;11:680-686.

70. Okamoto RJ, Wagenseil JE, DeLong WR, Peterson SJ, Kouchoukos NT, Sundt TM, III. Mechanical properties of dilated human ascending aorta. *Ann Biomed Eng.* 2002;30:624-635.

71. Mohan D, Melvin JW. Failure properties of passive human aortic tissue. I--uniaxial tension tests. *J Biomech.* 1982;15:887-902.

72. Vande Geest JP, Sacks MS, Vorp DA. Age dependency of the biaxial biomechanical behavior of human abdominal aorta. *J Biomech Eng.* 2004;126:815-822.

APPENDIX A

Faculty of Medicine
3655 Promenade Sir William Osler
Montreal, QC H3G 1Y6

Faculté de médecine
3655, Promenade Sir William Osler
Montréal, QC, H3G 1Y6

Fax/Télécopieur: (514) 398-3595

CERTIFICATION OF ETHICAL ACCEPTABILITY FOR RESEARCH INVOLVING HUMAN SUBJECTS

The Faculty of Medicine Institutional Review Board consisting of:

SERGE GAUTHIER, MD — FRANCES ABOUD, PHD

VINCENT GRACCO, PHD — MARIGOLD HYDE, BSC

LARA KHOURY, LL.B, BCL, PHD

has examined the research project **AØ6-M62-04B** entitled **"Geometric and Biomechanical Data for Modeling the Left Ventricular Outflow Tract and Proximal Coronary Arteries"**

as proposed by: Richard L. Leask (Applicant) to _____ (Granting Agency, if any)

and consider the experimental procedures to be acceptable on ethical grounds for research involving human subjects.

September 15, 2004 (Date) — _____ (Chair, IRB) — _____ (Dean of Faculty)

Institutional Review Board Assurance Number: FWA 00004545

INSTITUT DE CARDIOLOGIE DE MONTRÉAL

50 ANS d'histoires de cœur

ÉVALUATION D'UN PROJET
COMITÉ INTERNE DE LA RECHERCHE

Date de la réunion: 3 novembre 2004

No du projet: **04-729**

Investigateur principal: **Docteur Raymond Cartier**

Titre du projet: **Regional Characterization of Healthy and Diseased Human Ascending Aorta Tissue**

Décision du comité:

☐ 1 Approuvé sans modification.*

☒ 2 Approuvé mais une réponse aux commentaires ou aux questions est nécessaire.*

☐ 3 Projet acceptable, mais une réponse aux commentaires ou aux questions est nécessaire avant une approbation définitive.*

☐ 4 Problèmes majeurs identifiés, une révision majeure est nécessaire avant reconsidération.

☐ 5 Autre - voir ci-dessous.

Commentaires du comité:

Les investigateurs pourraient considérer demander à deux observateurs de faire l'évaluation semi-quantitative de la dégénérescence médiale.

Jean-Claude Tardif, MD, FRCPC, FACC
Président
Comité scientifique de la recherche
JCT:gb

Adressez vos réponses au Comité interne de la recherche, Secrétariat du Comité d'éthique.
*Le projet sera acheminé au Comité d'éthique pour évaluation de la déontologie.

c.c.: Mme Lise Courchesne

5000, rue Bélanger, Montréal (Québec) H1T 1C8 • Tél. : (514) 376-3330
Institut universitaire affilié à l'Université de Montréal